CERN 72-13
Laboratory I
Synchro-cyclotron
Machine Division
6 July 1972

ORGANISATION EUROPÉENNE POUR LA RECHERCHE NUCLÉAIRE
CERN EUROPEAN ORGANIZATION FOR NUCLEAR RESEARCH

PROTON TOTAL CROSS-SECTIONS ON ^{1}H, ^{2}D, ^{4}He, ^{12}C, AND ^{16}O IN THE ENERGY RANGE 180 TO 560 MeV

P. Schwaller, B. Favier, D.F. Measday,
M. Pepin, P.U. Renberg and C. Serre

GENEVA

1972

CERN 72-13
Laboratory I
Synchro-cyclotron
Machine Division
6 July 1972

ORGANISATION EUROPÉENNE POUR LA RECHERCHE NUCLÉAIRE

CERN EUROPEAN ORGANIZATION FOR NUCLEAR RESEARCH

PROTON TOTAL CROSS-SECTIONS ON ^{1}H, ^{2}D, ^{4}He, ^{12}C, AND ^{16}O IN THE ENERGY RANGE 180 TO 560 MeV

P. Schwaller*), B. Favier**), D.F. Measday***),
M. Pepin*), P.U. Renberg†) and C. Serre††)

This report was the subject of a thesis submitted to the
Swiss Federal Institute of Technology, Zurich, 1972.

G E N E V A

1972

---

*) Present address: SIN, Zurich, Switzerland.
**) Present address: University of Geneva, Switzerland.
***) Present address: University of British Columbia, Vancouver, Canada.
†) Present address: Gustaf Werner Institute, Uppsala, Sweden.
††) Present address: CERN, Geneva, Switzerland.

CERN - Service d'Information scientifique - H/506 - 2300 - juillet 1972

ABSTRACT

Proton total cross-sections on ^{1}H, ^{2}D, ^{4}He, ^{12}C, and ^{16}O have been measured in the energy range 180 to 560 MeV in a high precision transmission experiment with a statistical accuracy of ±0.2%. Random errors are typically ±0.5% for pp data, ±1% for ^{2}D and ^{4}He, and ±(1-3%) for ^{12}C and ^{16}O total cross-sections. Systematic errors of ±(0.8-1%) in the ^{1}H and ^{2}D data originate mainly from uncertainties in applying the correct Coulomb-nuclear interference corrections to the measured partial cross-sections before extrapolating to the total cross-section at zero solid angle.

The real parts of the nuclear spin-independent forward scattering amplitudes on ^{4}He, ^{12}C, and ^{16}O were obtained in the same experiment by analysing the angular dependence of the partial cross-sections in the Coulomb-nuclear interference region.

Total cross-sections are calculated in a Glauber-model approach, and the results are compared to this data.

CONTENTS

1. INTRODUCTION

In this report we discuss in detail a high precision transmission experiment performed at the CERN 600 MeV Synchro-cyclotron. The aim was to explore the forward direction when scattering protons on protons and on isospin zero nuclei (D, He, C, and O) in the range of 180 to 560 MeV incident kinetic energy.

The small-angle elastic scattering region is of considerable interest because it contains all the information on the spin-independent nuclear forward scattering amplitude f. The imaginary part of f is obtained when measuring the nuclear total cross-section and using the optical theorem. The real part is usually deduced from differential cross-section data in the Coulomb-nuclear interference region.

A transmission experiment measures partial cross-sections for several laboratory solid angles defined by successive circular transmission counters.

The total cross-sections are usually obtained by applying first the Coulomb and Coulomb-nuclear interference corrections to all partial cross-sections, and then extrapolating the corrected data to zero solid angle.

Each partial cross-section contains information on the elastic differential cross-sections in an integrated form. In particular, the Coulomb-nuclear interference effect contributes considerably to the partial cross-sections in the angular region where the Coulomb and nuclear amplitudes have similar orders of magnitude. With our high precision partial cross-section data we were able to analyse this region in order to deduce the real parts of the nuclear forward scattering amplitudes. The method was successful for the He, C, and O data; thus the complete forward amplitudes have been determined for these nuclei.

In general, total cross-section data are of great importance. Any model (optical model) in nuclear structure physics will use total cross-sections in order to determine unknown parameters (optical potentials); conversely, any theory without free parameters predicts total cross-sections which have to be compared to experimental data.

1.1 Nucleon-nucleon phase-shift analysis

There exists a unique set of phase shifts in the (I = 1) nucleon-nucleon system for energies up to about 450 MeV [1] (Livermore phase-shift analysis X). This analysis makes no use of pp total cross-section data as input, but predicts total nn cross-sections. Assuming charge symmetry to be valid, our pp data provide a direct test on these nn cross-sections and therefore on the reliability of the phases.

1.2 Glauber theory

Glauber theory has been very successful in describing elastic differential cross-sections at small scattering angles and high energies. It is interesting to search for the low-energy limit where the assumptions for the model are no longer valid. Surprisingly, the model still works when scattering pions of 100 to 300 MeV on nuclei. Very little has been done in nucleon-nucleus scattering at intermediate energies, since the theory becomes more complicated when spin effects have to be considered. Moreover, accurate experimental data are rather rare. We made an attempt to calculate p-D, He, C, and O total cross-sections with Glauber theory with the simplest possible assumptions, and have compared the results with our experimental data.

1.3 Forward dispersion relations

Forward dispersion relations in nucleon-nucleus scattering provide a powerful tool for exploring the unphysical region of such a system, provided that experimental total cross-section data and real parts of the forward scattering amplitude are available. In particular, FDR at intermediate energies are sensitive to mesonic exchange processes. Locher[2] has performed an extension of a low-energy FDR analysis on ^{4}He towards intermediate energies using our experimental data.

2. GENERAL PRINCIPLES OF THE EXPERIMENT

2.1 Transmission experiment

A simple and precise way of measuring the total cross-sections of protons on any target of interest is to perform a transmission experiment, i.e. to measure the attenuation of a proton beam in a block of target material:

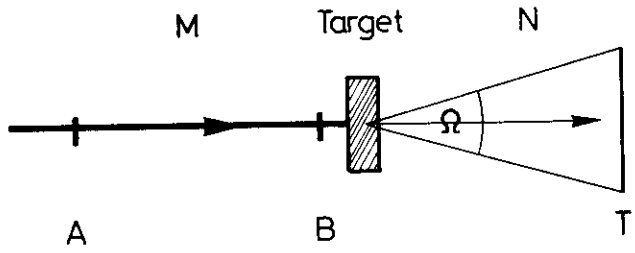

Fig. 1 Schematic principle of a transmission experiment

In Fig. 1 we define M, the number of protons incident on a target, given by a counter telescope AB, and N, the number of particles detected by the transmission counter T in coincidence with AB. Measuring M and N simultaneously, we can relate the transmission N/M to a partial cross section $\sigma(\Omega)$ with the formula

$$\frac{N}{M} = \varepsilon(1 - \delta)\, e^{-\sigma(\Omega)n} , \qquad (1)$$

where $\sigma(\Omega)$ is the cross-section per target nucleus for an incoming proton to be scattered outside the solid angle Ω,

n is the number of scatterers/cm^2 in the target,

ε the efficiency of counter T, and

δ the background absorption ($n = 0$) due to other scatterers in the beam line, such as air, target windows, the counter B, etc.

Denoting by the indices i and o two transmission measurements with the target "in" and "out", respectively, the transmission ratio R is given by:

$$R = \frac{(N/M)_i}{(N/M)_o} = e^{-\sigma(\Omega)n} . \qquad (2)$$

Thus one measures directly the partial cross-section $\sigma(\Omega)$, provided that the efficiency and background absorption suffer no change between the two measurements.

In reality, a change $\Delta\delta = \delta_i - \delta_o$ or $\Delta\varepsilon = \varepsilon_i - \varepsilon_o$ may occur and propagate to a systematic error in $\sigma(\Omega)$:

$$\frac{\Delta\sigma}{\sigma}(\Omega) = -\frac{1}{|\ln R|}\frac{\Delta R}{R} = -\frac{1}{|\ln R|}\left(\frac{\Delta\varepsilon}{\varepsilon} - \frac{\Delta\delta}{1-\delta}\right) \qquad (3)$$

$$\sim 10(\Delta\varepsilon - \Delta\delta)$$

for $R \sim 0.9$ (10% absorption in the target)

$\varepsilon \sim 1$

$\delta \sim 0$.

Given an accuracy $\Delta\sigma/\sigma$ of about 0.3% and an absorption of 10% in the target, $\Delta\varepsilon$ and $\Delta\delta$ should never exceed 0.03% unless such effects can be measured and therefore corrected within this precision. Possible sources are mentioned below, and appropriate tests are discussed in Section 3.6.

2.1.1 Background

The background absorption for a given experimental set-up depends on the beam energy. Since protons passing through the target lose a small fraction of their energy, the two transmission measurements, target "in" and "out" show different absorption behaviour in any material downstream of the target, especially in a set of successive transmission counters. A difference in beam shape, caused by multiple Coulomb scattering in the target, may also produce a slight change in the background absorption.

2.1.2 Efficiency

For a large counter, the efficiency depends on the position of impact of the particle. It is slightly higher near the edge than in the centre owing to variation of the pulse shape and therefore the timing characteristics. An effective efficiency in a transmission experiment is given by folding a beam intensity distribution $\tau(r)$ at the counter position with the efficiency $\varepsilon(r,\phi)$:

$$\bar{\varepsilon} = \frac{\int_0^{r_T} \tau(r) r \left[\int_0^{2\pi} \varepsilon(r,\phi)\, d\phi \right] dr}{2\pi \int_0^{r_T} \tau(r) r\, dr} \quad . \tag{4}$$

Since $\tau_i(r)$ and $\tau_o(r)$ differ considerably, $\bar{\varepsilon}_i$ can be higher than $\bar{\varepsilon}_o$, giving systematically too low a cross-section.

2.2 Statistical accuracy

The two numbers M = AB and N = ABT in a transmission experiment are strongly correlated since both coincidences measure the same particles. Fixing the monitor M in a preselection of the scaler system, the statistical fluctuations occur for (M - N), the number of particles scattered outside of counter T. We get

$$\Delta N = \pm \sqrt{M - N} \tag{5}$$

and therefore

$$\frac{\Delta(N/M)}{(N/M)} = \pm \frac{\sqrt{M - N}}{N} \quad . \tag{6}$$

For the two independent measurements i and o the relative error for the transmission ratio is given by

$$\frac{\Delta R}{R} = \pm \left[\frac{M_i - N_i}{N_i^2} + \frac{M_o - N_o}{N_o^2} \right]^{\frac{1}{2}} \quad . \tag{7}$$

With Eq. (2) it leads to a relative error

$$\frac{\Delta\sigma}{\sigma} = \frac{1}{|\ln R|} \frac{\Delta R}{R} \quad . \tag{8}$$

For a given statistical accuracy $\Delta\sigma/\sigma = \pm 0.2\%$ and a background absorption $\delta = 1.5\%$, the minimum number of monitor counts M_i and M_o in function of R is plotted in Fig. 2. In order

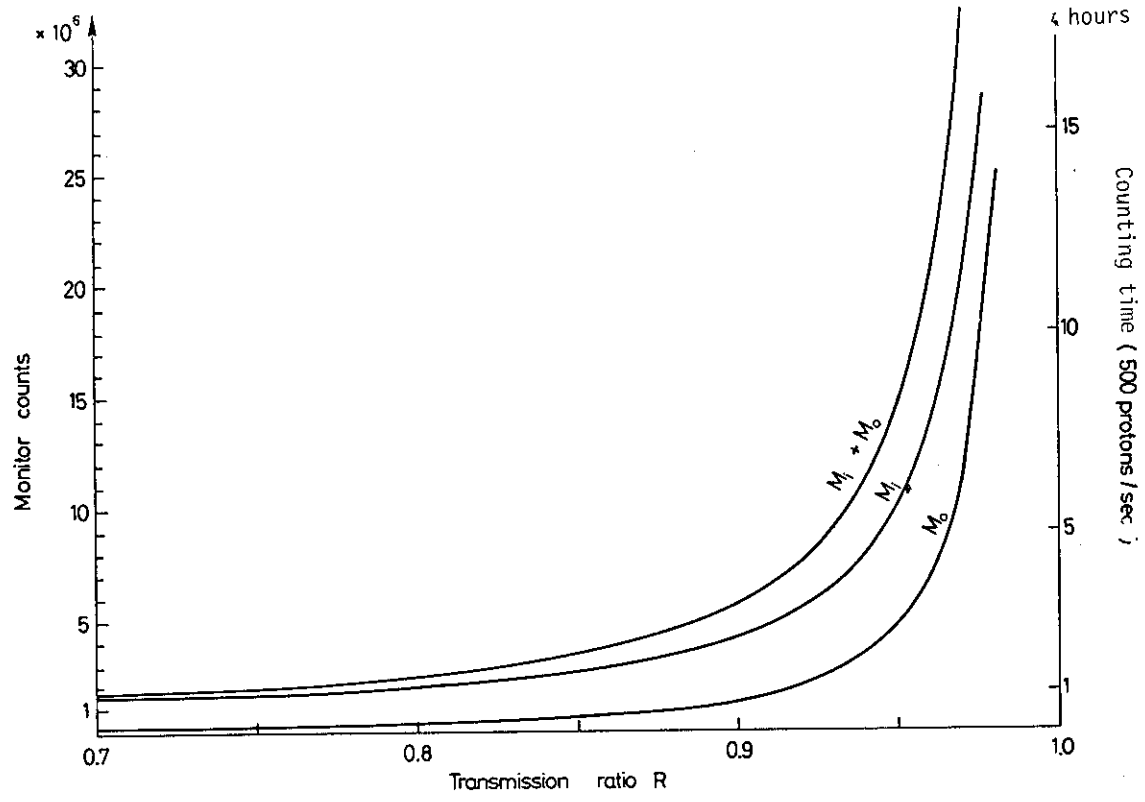

Fig. 2 Monitor counts and counting time as a function of transmission ratio R for a given statistical accuracy $\Delta\sigma/\sigma = \pm 0.2\%$ and a background absorption δ of $\pm 1.5\%$

to have only a few hours of counting time, a minimum target absorption A = 1 - R of about 8% is required.

2.3 Data analysis*)

The nuclear total cross-section is defined as the sum of total nuclear elastic and reaction cross-sections

$$\sigma_{tot} = \sigma_{ne} + \sigma_r \ . \tag{9}$$

The partial cross-section for small solid angles Ω measures the quantity

$$\sigma(\Omega) = \int_{\Omega}^{4\pi} \left(\frac{d\sigma}{d\Omega}\right)_{el} d\Omega + \left[\sigma_r - \int_{0}^{\Omega} \left(\frac{d\sigma}{d\Omega}\right)_{inel} d\Omega\right] , \tag{10}$$

where

$$\left(\frac{d\sigma}{d\Omega}\right)_{el} = \left(\frac{d\sigma}{d\Omega}\right)_{C} + \left(\frac{d\sigma}{d\Omega}\right)_{ne} + \left(\frac{d\sigma}{d\Omega}\right)_{Cni} \tag{11}$$

*) The following notation is used for the cross-sections:

ne	= nuclear elastic	C	= Coulomb
el	= elastic	Cni	= Coulomb-nuclear interference
inel	= inelastic	r	= reaction

and $(d\sigma/d\Omega)_{inel}$ stands for the differential cross-section for the production of *charged* secondaries.

Using the formulas (9), (10) and (11) $\sigma(\Omega)$ is related to the total cross-section by:

$$\sigma(\Omega) = \sigma_{tot} - \int_0^{\Omega} \left[\left(\frac{d\sigma}{d\Omega}\right)_{ne} + \left(\frac{d\sigma}{d\Omega}\right)_{inel} \right] d\Omega + \left[\kappa(\Omega, n) + \int_{\Omega}^{4\pi} \left(\frac{d\sigma}{d\Omega}\right)_{C} d\Omega \right] + \int_{\Omega}^{4\pi} \left(\frac{d\sigma}{d\Omega}\right)_{Cni} d\Omega \ . \qquad (12)$$

The term $\int_0^{\Omega} \left[(d\sigma/d\Omega)_{ne} + (d\sigma/d\Omega)_{inel}\right] d\Omega$ represents the fraction of all charged particles scattered elastically by strong interaction or produced in an inelastic reaction and detected in the transmission counter T.

$\int_{\Omega}^{4\pi} (d\sigma/d\sigma)_C \, d\Omega$ is the particle loss caused by single Coulomb scattering; κ is a multiple Coulomb scattering correction for n scatterers.

$(d\sigma/d\Omega)_{Cni}$ in the last integral takes care of the interference between the Coulomb amplitude f_C and the nuclear spin non-flip amplitude f_{ne} in a (pX) system and is given by

$$\left(\frac{d\sigma}{d\Omega}\right)_{Cni} = 2\{\mathrm{Re}\ f_C\ \mathrm{Re}\ f_{ne} + \mathrm{Im}\ f_C\ \mathrm{Im}\ f_{ne}\} \ . \qquad (13)$$

It is positive (negative) for constructive (destructive) interference. Since f_C is essentially real, Re $f_C \cdot$ Re f_{ne} provides the dominant contribution to the interference integral. However, Re f_{ne} is at present poorly known in the energy range we are considering.

For a set of partial cross-sections $\sigma(\Omega_i)$, measured simultaneously with an array of successive transmission counters T_i with different solid angles Ω_i, the total cross-section σ_{tot} is obtained by first correcting all the partial cross-sections by the Coulomb and interference terms, and extrapolating the corrected data to zero solid angle with a polynomial of first or second order in Ω. The choice for an appropriate interval of solid angles covered by the transmission counters is rather important for the precision of σ_{tot}.

Equation (12) is applied for a kinetic energy E_c in the centre of the target and a solid angle Ω given by the mean over the target length ℓ:

$$\Omega = \bar{\Omega} = \frac{1}{\ell} \int_{-\ell/2}^{+\ell/2} \Omega(x + d)\, dx \qquad (14)$$

(d = distance from the target centre to the transmission counter).

We can use this approximation (Eq. 12) provided that σ_{tot} as well as all integrals remain linear as a function of E and Ω in the intervals

$$E_c - \frac{\Delta E}{2} \le E \le E_c + \frac{\Delta E}{2} \ ,$$

and

$$\bar{\Omega} + \frac{\Delta\Omega}{2} \ge \Omega \ge \bar{\Omega} - \frac{\Delta\Omega}{2} \ .$$

ΔE is the energy loss of protons through the target and $\Delta\Omega$ the difference between the maximum and minimum solid angles as a consequence of finite target length.

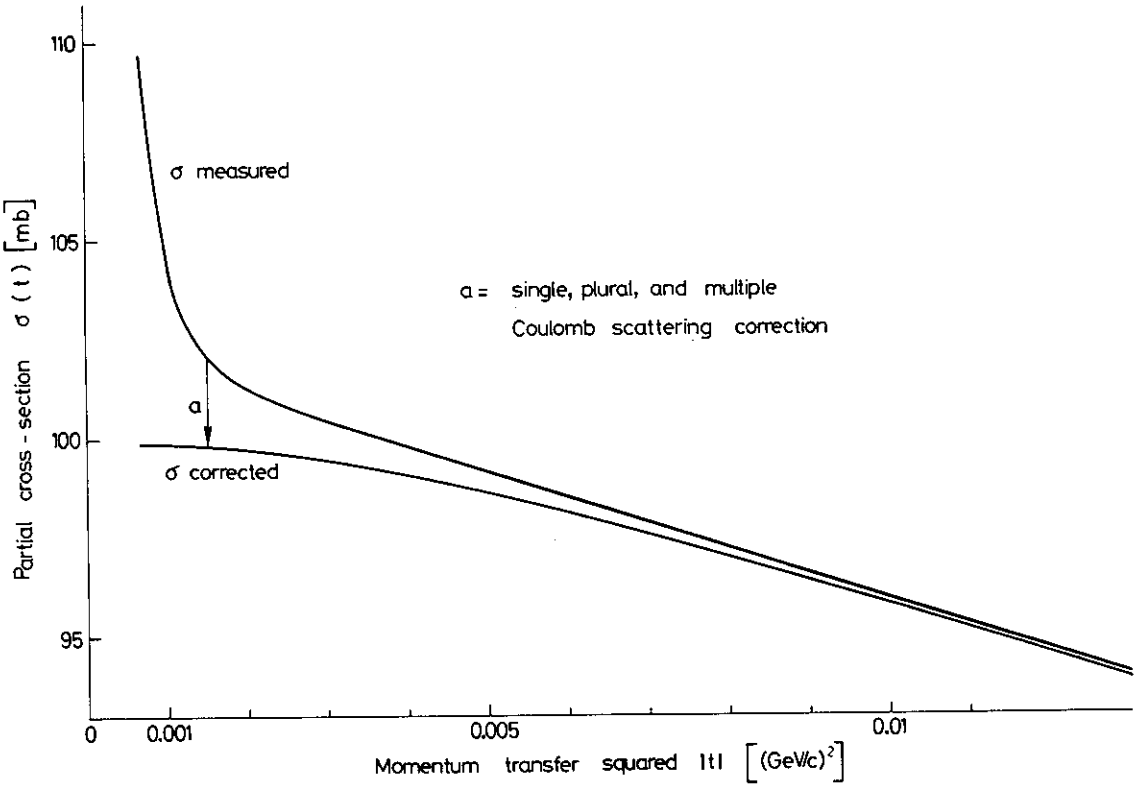

Fig. 3 Typical shape of partial cross-sections as a function of $|t|$

Figure 3 shows the typical shape of partial cross-sections as a function of momentum transfer squared $|t|$:

$$t = -\frac{k^2}{\pi}\,\Omega(\text{c.m.}) = -2k^2(1-\cos\theta_{\text{c.m.}}) \qquad k = \text{c.m. momentum}. \tag{15}$$

The t-dependences of differential cross-sections and their integrals in Eq. (12) explain the structure of this curve.

Table 1

	$(d\sigma/dt)$	$\int(d\sigma/dt)\,dt$
Coulomb	$1/t^2$	$1/\lvert t\rvert$
Interference	$\pm\, 1/\lvert t\rvert$	$\pm \ln \lvert t\rvert$
Nucl. elastic	$e^{-\gamma^2\lvert t\rvert} \sim 1 - \gamma^2\lvert t\rvert$	$t + \gamma^2(t^2/2)$
Inelastic	We assume it is constant for small angles*)	t

*) There exists some experimental evidence that the cross-sections of reaction products follow a Gaussian distribution as a function of the scattering angle θ, of which the characteristic angle at half-height is $\theta_{\frac{1}{2}} \sim 28°$ [3,4] in the energy range of interest.

The Coulomb term dominates all the other integrals at very small angles $[|t| < 0.001\ (\mathrm{GeV/c})^2]$ causing a big correction, but falls off rather fast with increasing $|t|$. The structure of the interference term becomes important in the interval $0.001 < |t| < 0.01\ (\mathrm{GeV/c})^2$. The integrals of the strong interaction cross-sections are polynomials of second order in t, but essentially behave linearly for $|t| < \sim 0.005\ (\mathrm{GeV/c})^2$. Partial cross-sections corrected by the pure Coulomb term ($\sigma_{\text{corrected}}$ in Fig. 3) have a t-dependence of the form

$$\sigma_{\text{corr}}(t) \simeq \sigma_{\text{tot}} + c_1 t + c_2 \ln\left(\frac{t}{t_{\text{max}}}\right) \tag{16}$$

$$t_{\text{max}} = -4k^2$$

in the interval

$$0.001 < |t| < 0.005\ (\mathrm{GeV/c})^2 .$$

c_2 is the strength of the second derivative of the curve and represents, apart from known constants in the Coulomb amplitude, the real part of the nuclear scattering amplitude averaged over the above t-interval.

The curvature of σ_{corr} in Fig. 3 is typical for destructive interference

$$\left(\frac{d^2\sigma_{\text{corr}}}{dt^2} = -\frac{c_2}{t^2} < 0\right) .$$

In the absence of Coulomb nuclear interference, $\sigma_{\text{corr}}(t)$ would thus be quite well approximated by a straight line.

With this qualitative description it becomes clear that a transmission experiment yields total cross-sections and, as a second-order effect, the real part of the nuclear forward scattering amplitude, provided that the partial cross-sections are measured precisely enough in the region where the Coulomb nuclear interference is important.

2.4 Proton beams and their energies

To supply the protons of different energies required to measure the energy dependence of total cross-sections, one can utilize a variable energy cyclotron or one can degrade the proton beam of a fixed energy synchro-cyclotron.

Proton total cross-sections on nuclei do not show any resonance structure in the energy range 200-600 MeV and vary rather slowly. Therefore beam energies need not be measured with high precision; an error of ±3 MeV is equivalent to an error in the cross-section scale of at most ±0.5%. This energy precision can be achieved by using a differential range curve technique as described in Section 3.7.

3. EXPERIMENTAL DESIGN

3.1 Proton beams

The experimental layout at the 600 MeV Synchro-cyclotron at CERN is shown in Fig. 4.

The energy variation of protons between 400 and 600 MeV was achieved by degrading a scattered-out beam produced on an internal target in the SC. To get energies below 400 MeV, a higher intensity incident on the degrader was required and obtained by sharing the internal proton beam, i.e. extracting about 20% directly.

Boron carbide (B_4C) was used as degrading material; it is best suited for three reasons:

i) the low effective charge Z keeps beam losses due to Coulomb scattering reasonably small;

ii) owing to its rather high density of 2.5 g/cm^3, only about 15 cm of B_4C are needed to reduce the proton energy by 100 MeV; thus 200 MeV was reached with 60 cm degrader length;

iii) it has a low residual activity and can be handled soon after irradiation by the proton beam.

The beam was refocused by two quadrupole lenses, collimated in the shielding wall, analysed in a bending magnet, and defined with two counters A and B in coincidence. Both counters were 3 cm in diameter, 3 mm thick, and placed 3 m apart. An additional collimator after counter A with an aperture of 5 cm diameter was used to stop all particles missing counter A; thus it reduced the counting rate in the big transmission counters T_i.

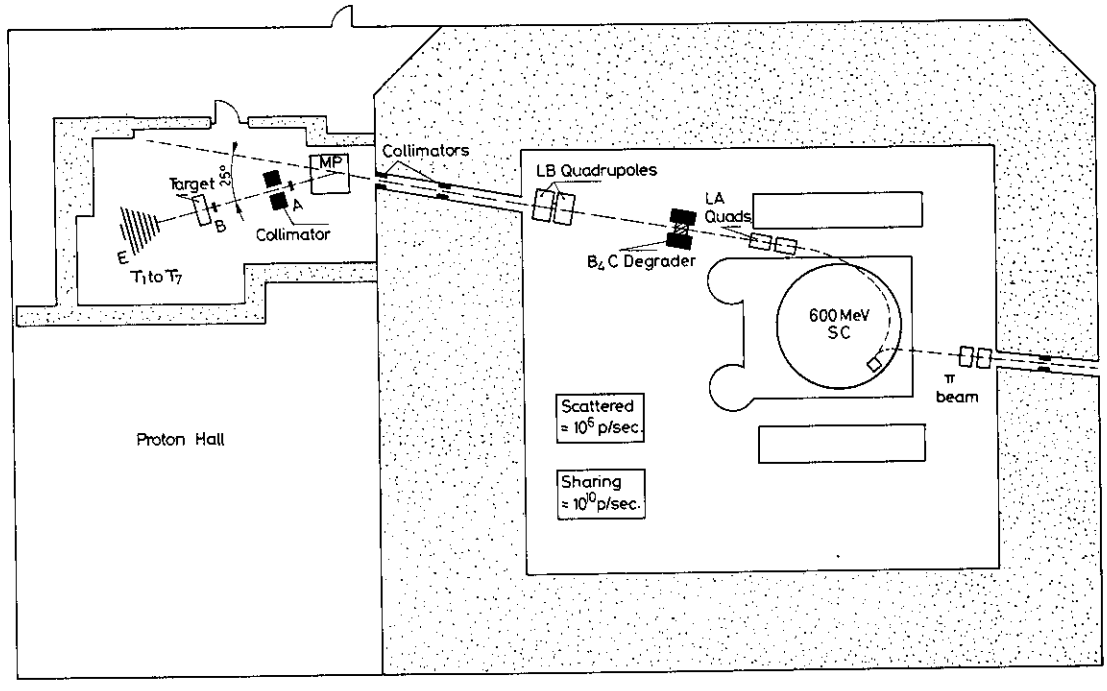

Fig. 4 Experimental layout

3.2 Targets

The target length, a very important parameter, must be a compromise between contradictory requirements:

i) Targets should be as thin as possible in order to satisfy the condition that all terms in Eq. (12) are linear in energy E and solid angle Ω within the intervals ΔE and $\Delta\Omega$ given by the target length; in addition, a short target keeps the plural and multiple Coulomb scattering correction small; the multiple nuclear scattering correction is then negligible.

ii) Thick targets are desired in order to keep down the time for data-taking, given a statistical accuracy on partial cross-sections of 0.2% (see Fig. 2). In addition, the high precision of the background transmission experiment becomes less decisive a condition the bigger the target absorption is, i.e. the smaller the ratio $\delta/1-R$.

All targets had absorptions ranging from 8% to 15%, the background absorption being always about 1.5% (see Table 2). The liquid target containers, such as those for H_2, D_2, and He (Fig. 5), consisted of metal cylinders, 16 cm in diameter, with 0.25 mm thick mylar windows at both ends. Concentric copper cylinders with 15 cm diameter were mounted inside the liquid, and prevented bubbles produced on the outer walls from traversing the useful portion of the target. Thermal screens at liquid-nitrogen temperature surrounded the target at half distances to the cryostat vessel; these reduced the heat input considerably, resulting in an evaporation loss of liquid H_2 and He of 0.1 ℓ/h and 1 ℓ/h, respectively.

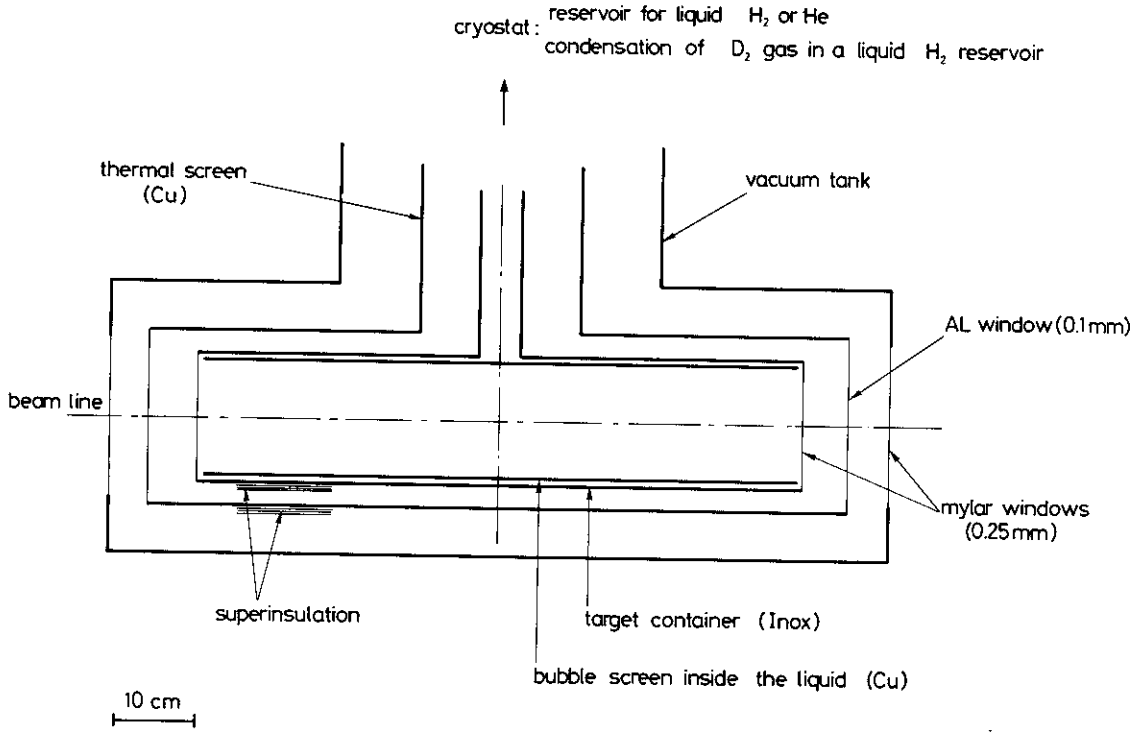

Fig. 5 Sketch for liquid H_2, D_2, and He targets. A target, 75 cm long, was used for H_2 and He in turn. D_2 gas was condensed in a liquid H_2 reservoir of a separate cryostat and filled into a target of 35 cm length

Target densities were determined by measuring the vapour pressure of hydrogen and helium immediately above the liquid, and converting it into densities by means of tables[5,6].

The temperature of liquid deuterium was measured with a hydrogen gas thermometer. It was mounted inside the liquid, immediately above the target container. The observed temperatures varied between 21.4°K and 22.3°K, depending on whether the liquid hydrogen reservoir (20.4°K), the condenser of deuterium gas, was completely full or almost empty. Again, liquid-deuterium densities were obtained using the above-mentioned conversion table[5].

The target lengths were measured carefully at liquid-nitrogen temperature as a function of pressure in the vessel. A very small folding correction (0.2 mm) caused by the curvature of the windows together with a given beam shape had to be applied.

Oxygen total cross-sections were measured in a water target of 8.7 cm length and 16 cm diameter.

Values and estimated errors of all parameters of interest are listed in Table 2.

Dummy targets were used in the background transmission measurements. Systematic differences between dummy and empty target background absorptions of at most 0.03% were observed and the corresponding corrections applied to the total cross-sections.

Table 2

Target parameters

Element	H_2	D_2	^4He	^{12}C	^{16}O (H_2O)
Target length ℓ (cm)	75	35	75	5	8.7
$\Delta\ell/\ell$ (%) ±	0.2	0.3	0.2	0.1	0.25
Thickness th (g/cm^2)	5.3	5.9	9.3	9.2	8.7
$\Delta th/th$ (%) ±	0.21	0.5	0.21	0.15	0.3
Absorption (%)					
200 MeV	7	10	13	12	11
550 MeV	10	11	15	13	11
Energy loss ΔE (MeV)					
200 MeV	52	25	37	38	40
550 MeV	29	15	23	21	24

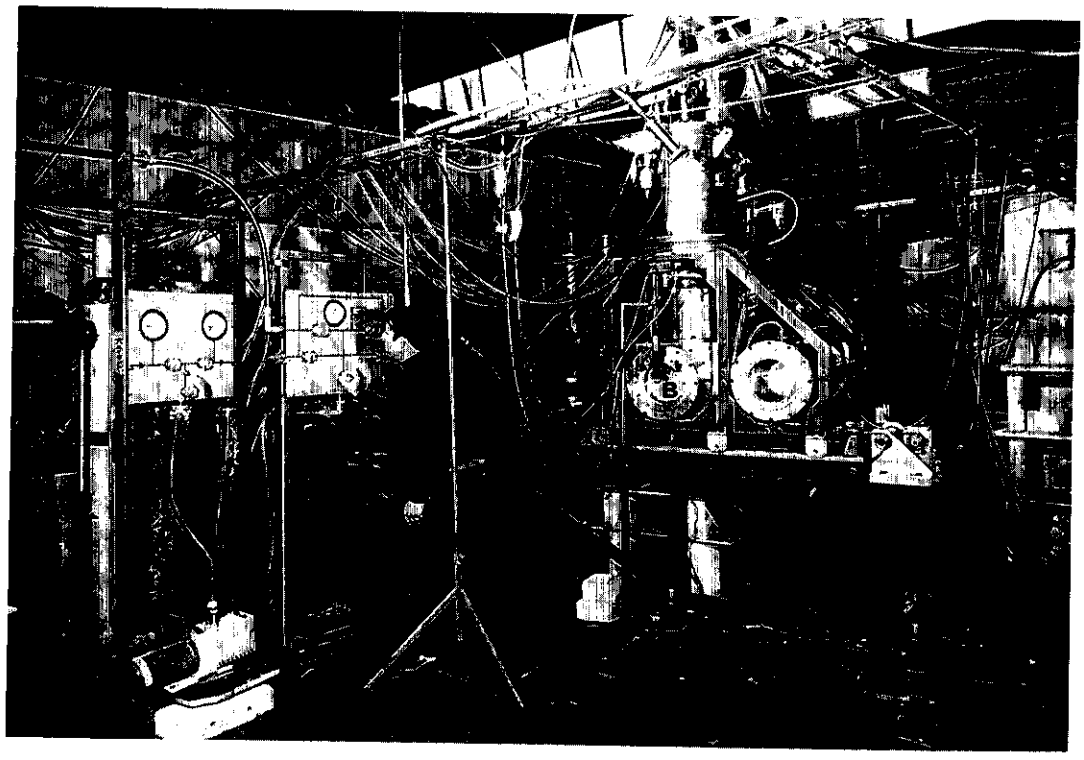

Deuterium target. Target and dummy target, sitting on a trolley, could be positioned in turn in the beam line by remote control. The second beam-defining counter (B) is placed close to the targets.

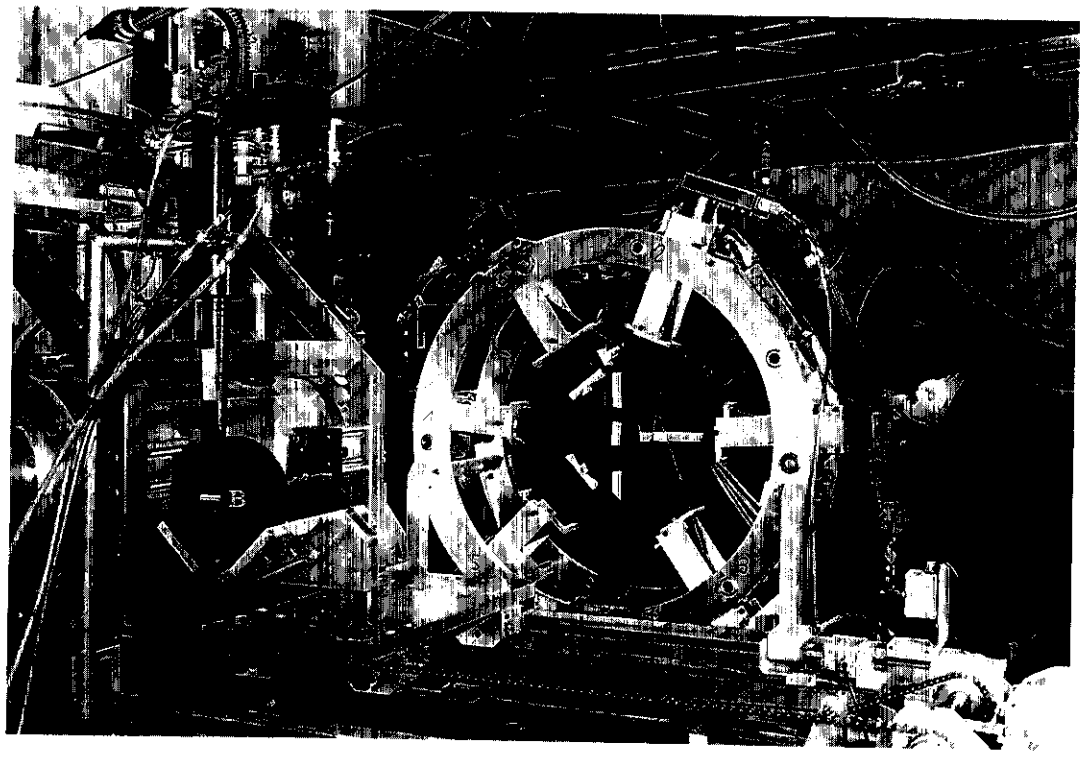

Transmission counters 1 to 7 are mounted on the support. The small counter (B) in front of the carbon target defines the incident beam.

3.3 Transmission counters

Seven circular transmission counters, 5 mm thick, were mounted on a trolley. They covered solid angles in the sequence 1, 2, 3, 4, 5, 7, 9, the smallest and largest counters being 15 cm and 45 cm in diameter, respectively.

The whole assembly could be displaced on rails along the beam line. The alignment was achieved by scanning the beam at the transmission counter position with a small scintillator in coincidence with the monitor AB, thus defining the beam centre line. The solid angle covered by each counter was calculated as a mean over the target length ℓ:

$$\bar{\Omega} \cong \Omega_{\substack{\text{target}\\ \text{centre}}} \left[1 + \left(\frac{\ell}{2d} \right)^2 \right] , \tag{17}$$

where d is the distance from the transmission counter to the target centre. Any correction due to a finite beam size was negligibly small.

3.4 Electronics

The fast electronic logic shown in Fig. 6 consisted of standard NIM shapers and coincidence units and a SEN 300 scaler system (100 MHz). The pulses from the NIM shapers were between 4 and 6 nsec long, giving a resolution time in the coincidences of about 10 nsec. For a preselected number of monitor counts M = AB, all coincidences ABT_i (i = 1, ..., 7) were recorded simultaneously. A small counter E at the very back of the transmission counter assembly in coincidence with the monitor M measured the efficiency $\varepsilon = ABT_iE/ABE$ in the centre of each counter T_i. For data-taking it never dropped below 99.97%.

Accidental effects were measured in the coincidences AB and MT_i by delaying one of the coincidence signals by 60 nsec, corresponding to the time delay between two beam pulses in

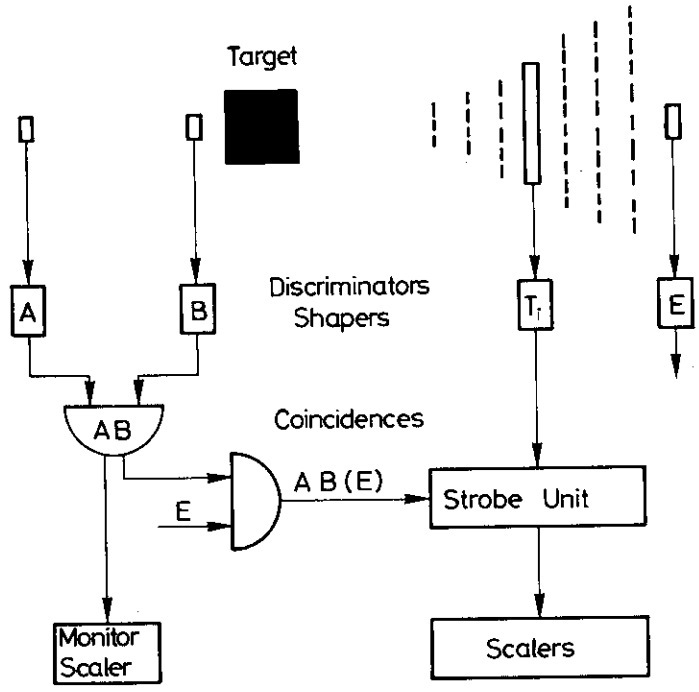

Fig. 6 Fast electronic logic

the microstructure of the synchro-cyclotron. The accidental counts never exceeded 0.2% of the real coincidences. Two protons passing simultaneously through the beam-defining telescope AB are detected as one particle only. They cause an error in the transmission ratio R if only one of them hits the transmission counter and the other is scattered out by the target. A systematic small correction was applied to all total cross-sections increasing them by

$$\frac{\Delta\sigma_{tot}}{\sigma_{tot}} \simeq + \text{acc} \; \frac{1 - R}{\ln R} \simeq \text{acc} \; ,$$

where acc = $AB_{delayed}/AB$.

Efficiencies and accidental rates are sensitive on intensity and duty cycle of the proton beam. Therefore running intensities of less than 1000 p/sec in AB were used to reach the highest efficiency and the lowest accidental rate.

3.5 Data-taking

For each element and energy, transmission experiments were performed for two different distances between target centre and transmission counter array. This allowed us to cover the full interval of interest:

$$0.001 < |t| < 0.01 \; (\text{GeV/c})^2 \; .$$

It also provided a cross check for systematic effects in the partial cross-sections when different transmission counters covered the same solid angle Ω.

The seven partial cross-sections at a fixed geometry, measured simultaneously, are strongly correlated, since in first approximation all counters record the same particles. Therefore, the statistical errors do not reduce when fitting any curve through these cross-sections in order to extrapolate to zero solid angle. By this argument the total number of monitor counts M required to achieve a given statistical accuracy is that given in Section 2.2, irrespective of the number of individual measurements performed in an experiment.

3.6 Tests of systematic effects

Many tests were carried out in order to identify possible systematic errors.

In particular, careful attention was given to any change of background absorption between target "in" and "out" measurements. To investigate this, we doubled this background absorption by inserting additional material in the beam line, in one case between counter B and the target, and in another test immediately in front of the transmission counters. Any systematic change in partial cross-sections fell within statistical errors and therefore was negligible.

However, the background absorption, being different for each transmission counter T_i, depends on the kinetic energy of protons hitting the transmission counter array, and can be different for target "in" and "out" since the target itself causes an energy change. A usual target "out" experiment was compared with a background absorption obtained by degrading the proton beam in the SC machine hall with an additional block of material giving an energy loss equal to that of the target. We found that the correction to the partial cross-sections was negligible for the smallest transmission counter, which was closest to the target, but

increased towards the big counters. Figure 7 shows, as an example, that the correction applied depends linearly on the solid angle Ω with a bigger slope at low energies, and extrapolates to a small correction at zero solid angle.

In order to confirm that the finite beam size (3 cm diameter) introduced no systematic errors, we replaced the normal beam-defining counters by 1×1 cm^2 counters. Only the partial cross-sections at very small angles [$|t| < 0.001$ (GeV/c)^2], right in the Coulomb peak, were affected. (These angles are not used in the final extrapolation of the data.)

In a further test we purposely displaced the transmission counters 1 cm off the beam line. It showed that the alignment procedure was sufficiently precise.

As an alternative to the electronic scheme in Fig. 6, we checked whether the transmission ratio R_i changes when recording MT_iT_{i+1} instead of MT_i only. This requirement of a coincidence between two successive transmission counters eliminates the counts due to Čerenkov light pulses in the light-guides of the counters. A systematic increase of less than 0.1% in the total cross-section was observed. As a control, MT_1T_2 and MT_6T_7 were always measured.

While observing the accidental rates, the beam intensity was regulated with great care in order to reduce dead-time effects in the electronics and to reach an efficiency of 99.97% at the centre of each counter for the worst case. Since the efficiency does not increase substantially towards the edge of the counters, we estimate that systematic errors on total cross-sections due to any change of effective efficiency (defined in Section 2.1) between target "in" and "out" never exceeded 0.1%.

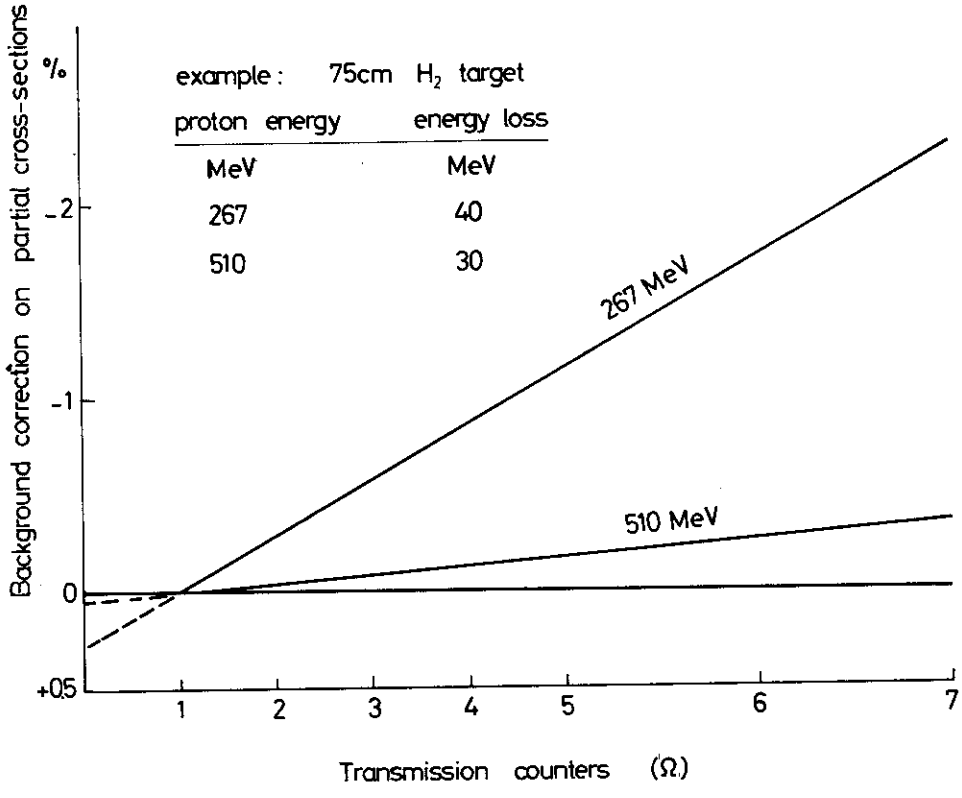

Fig. 7 Background corrections

3.7 Range energy measurement

As a simple method of deriving the mean energy of the proton beam, we used the differential range curve technique illustrated in Fig. 8.

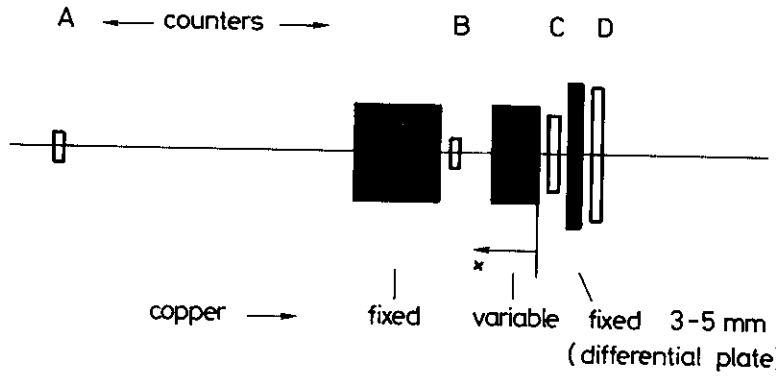

Fig. 8 Layout for range-energy measurement

It consisted of recording the number of protons ABC$\bar{D}$ stopped in a thin "differential" copper plate for a given monitor AB as a function of the effective copper length; particles had to traverse the following amount of material: Fixed + variable Cu + counters B and C + half the differential plate.

Figure 9 illustrates that this method measures the slope of an integral range curve ABC/AB and gives a rather sharp peak when reaching the range of protons in Cu. The ratio of peak-height to background below the peak is biggest if the variable Cu length x covers only the interval where the peak occurs. The mean kinetic energy of the proton beam incident

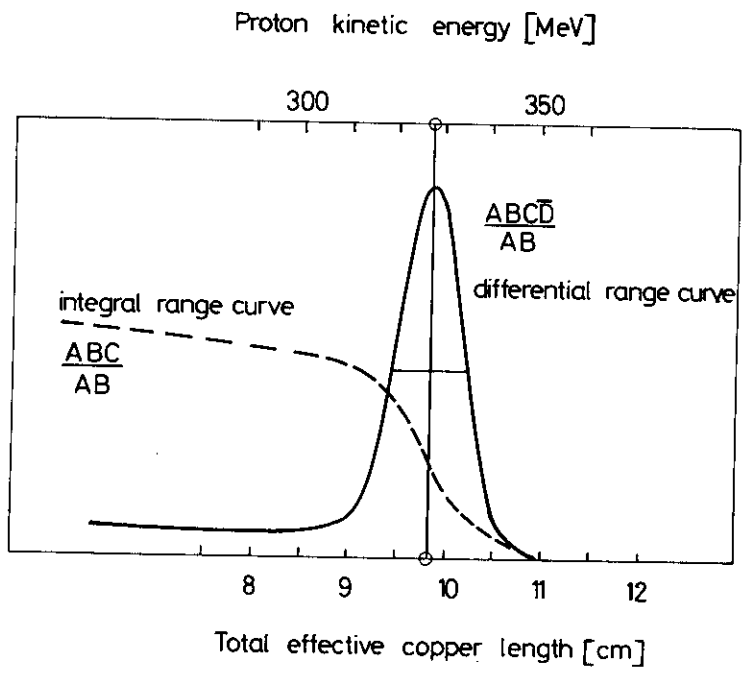

Fig. 9 Typical integral and differential range curve

on the target is found from the position of the peak using range-energy tables; it can be determined to within ±2 MeV. We used the range-energy tables of Serre[7] which agree to within the claimed error with those of Janni[8] and of Barkas and Berger[9].

The energy resolution of the system is essentially defined by the thickness of the differential copper plate ($\Delta E_{res} \sim 8$ MeV). Unfolding the measured peak full width at half height ΔE_m, the energy width of the beam ΔE_b can be approximated by

$$\Delta E_b \sim (\Delta E_m^2 - \Delta E_{res}^2)^{\frac{1}{2}}$$

and was found to be always within the limits

$$12 \text{ MeV} < \Delta E_b < 20 \text{ MeV}$$

in agreement with estimated energy widths expected from the analysing power of the bending magnet, $\Delta p/p \sim \Delta\phi/\phi$ ($\phi = 25°$ bending angle; $\Delta\phi$ is given by the beam-defining counter B and the diameter of the collimator hole at the exit of the shielding wall).

In order to get an idea of possible systematic errors in this method, we performed a floating-wire experiment. The trajectory of a charged particle through a magnet can be simulated with a thin wire that carries a d.c. current I and is subject to a tension K. If the wire coincides outside any fringe field $\vec{B}$ of the magnet with the beam centre line, the ration K/I is a direct measure of the quantity $\int_{wire} \vec{B} \times d\vec{\ell}$ ($d\vec{\ell}$ = element of the wire) and leads to the momentum by the formula

$$p(\text{MeV/c}) = \frac{K(g^*)}{I(A)}\ 2.9389 \ .$$

A systematic discrepancy of at most 3 MeV was observed between the floating-wire technique and the range curves.

4. DATA EVALUATION

All measured partial cross-sections were analysed in two steps:

i) The fraction of incoming protons scattered outside the solid angle Ω by single, plural, and multiple Coulomb interaction was calculated and the correction applied to each partial cross-section $\sigma(\Omega)$.

ii) The Coulomb-nuclear interference effect and the extrapolation to zero solid angle were treated differently for light elements (H and D) and for heavier elements (He, C, O respectively, for reasons mentioned below.

4.1 Single, plural, and multiple Coulomb scattering correction

4.1.1 Single Coulomb scattering

The single scattering correction in Eq. (12) results from

$$\Delta\sigma_C(t) = -\int_{t}^{t_{max}} \left(\frac{d\sigma}{dt}\right)_C (t')\, dt' \ , \qquad (18)$$

where

$$\left(\frac{d\sigma}{dt}\right)_C = 4\pi\left(\frac{Z}{\beta}\right)^2 \left(\frac{e^2}{\hbar c}\right)^2 \frac{1.9733^2}{10\ t^2} F^2(t) \qquad \left[\text{mb}/(\text{GeV}/c)^2\right] \qquad (19)$$

is the Rutherford cross-section multiplied by the charge from factor squared of the scatterer;

Z = charge of the scatterer;

β = laboratory velocity of the incoming proton;

$e^2/\hbar c \simeq 1/137$ is the fine structure constant;

$|t|$ = momentum transfer squared in $(\text{GeV}/c)^2$;

$F(t)$ = form factor of the scatterer. This is taken to have the form

$$F(t) = e^{-(R^2/6)\cdot|t|} \ .$$

We used the following charge r.m.s. radii R

Table 3

Target	^{1}H	^{2}D	^{4}He	^{12}C	^{16}O
R (fermi)	*	2.8 a)	1.67 b)	2.4 c)	2.54

*) The form factor in the pp data evaluation was neglected.

a) V. Franco and R.J. Glauber, Phys. Rev. 142, 1195 (1966).

b) R.F. Frosch, J.S. McCarthy, R.E. Rand and M.R. Yearian, Phys. Rev. 160, 874 (1967).

c) H.A. Bethe, Ann. Phys. 3, 190 (1958).

4.1.2 Multiple Coulomb scattering

As a second-order effect we considered a plural and multiple Coulomb scattering correction due to successive scatterings of protons traversing the target. This is important at small scattering angles where the Rutherford cross-section varies most rapidly. An appropriate way of calculating this correction is to apply Molière's multiple scattering theory[10-12].

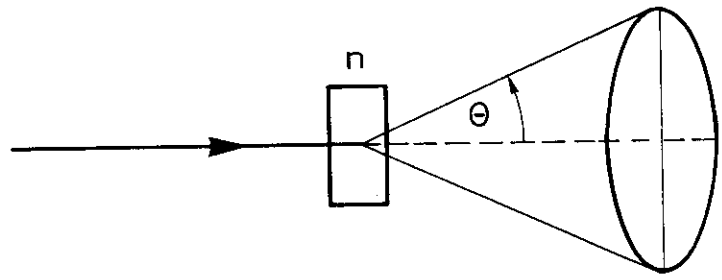

The probability dP for a proton incident on a target of n atoms/cm^2 to be scattered into a solid angle element $d\Omega = 2\pi\ \theta\ d\theta$ of a cone of small aperture is given by

$$dP(\theta) = f_M(\theta)\ d\Omega = 2\pi\ f_M(\theta)\ \theta\ d\theta\ , \tag{20}$$

where $f_M(\theta)$ is the Molière probability density distribution. To an accuracy of one per cent, Molière gives the angular distribution of f_M by the sum of three analytic terms. It is completely determined by an expansion parameter B and an angle χ_c:

$$dP(\eta) = \eta\ d\eta \left[f_0(\eta) + \frac{1}{B}\ f_1(\eta) + \frac{1}{B^2}\ f_2(\eta) \right] \tag{21}$$

where

$$\eta = \frac{\theta}{\chi_c \sqrt{B}} \quad \text{dimensionless}$$

$f_k(\eta)$ are Bessel transforms

$$f_k(\eta) = k!^{-1} \int_0^\infty u\ du\ J_0(\eta u) \exp\left(-\tfrac{1}{4}u^2\right) \left[\tfrac{1}{4}u^2 \ln\left(\tfrac{1}{4}u^2\right)\right]^k\ , \quad (k = 0,\ 1,\ 2) \tag{22}$$

where $f_0(\eta)$ is simply $2e^{-\eta^2}$.

These Bessel transforms were calculated by Marmer[13], but there is an error in the tabulation of f_0. The first term in brackets in Eq. (21) is the well-known Gaussian, while the second term goes over into the single scattering Rutherford formula at large angles, and the third term is a correction in the intermediate region.

Molière calculates his distribution $f_M(\theta)$ with two characteristic angles χ_c and χ_a, B being a function of these, as explained later.

a) χ_c is defined by the equation

$$n \int_{\chi_c}^\infty \left(\frac{d\sigma}{d\Omega}\right)_C 2\pi\ \chi\ d\chi = 1 \tag{23}$$

and reflects essentially the target thickness

$$\chi_c^2 \sim n\, Z^2 .$$

The extension of the upper integration limit (π) to ∞ is mathematically convenient in order to get a sensible normalization of the Molière distribution. However, it is physically irrelevant since we are concerned with a small-angle approximation and $(d\sigma/d\Omega)_C$ is strongly peaked forward.

b) A screened Coulomb potential of the form $U(r) \sim (Z/r)\, e^{-r/a}$ leads by Born approximation to the differential cross-section

$$\frac{d\sigma}{d\Omega}(\theta) \sim \frac{Z^2}{(\chi_a^2 + \theta^2)^2} , \tag{24}$$

where χ_a, the screening angle, describes the scattering atom. It prevents the cross-section at very small scattering angles $\theta \lesssim \chi_a$ from reaching infinity:

$$\chi_a \sim \frac{\lambda}{a} ,$$

where λ is the de Broglie wavelength of the incoming proton ($\simeq$ 0.15 - 0.25 fermi in this experiment); a depends on a model for the electron distribution around the nucleus, and is proportional to $Z^{-1/3}$ in the Thomas-Fermi statistical model and equal to about 10^5 fermi. Hence

$$\chi_a \simeq 10^{-3} \text{ mrad} \ll \chi_c \simeq 1 - 5 \text{ mrad for all targets} .$$

The Coulomb total cross-section using formula (24) is given by

$$\sigma_C = \int_0^\infty \left(\frac{d\sigma}{d\Omega}\right) d\Omega \sim \frac{Z^2}{\chi_a^2} \sim Z^{4/3} . \tag{25}$$

For the mean number of collisions in the target, one obtains

$$\mu = n\, \sigma_C \sim \rho \cdot \ell\, \frac{Z^{4/3}}{A} \sim \left(\frac{\chi_c}{\chi_a}\right)^2 . \tag{26}$$

It is interesting to see that $Z^{4/3}/A$ is always of the order 1. Therefore $\mu/\rho\cdot\ell$, the mean number of collisions per g/cm^2, is nearly the same for all elements and is about 10,000.

The expansion parameter B in Eq. (21) is directly related to μ by the expression

$$\frac{e^B}{B} \equiv \mu , \tag{27}$$

and B is typically between 14 and 20 for all targets.

The fraction of particles scattered outside the transmission counter T_i is

$$\int_{\theta=\theta_i}^{\infty} f_M(\theta')\, 2\pi\, \theta'\, d\theta' = 1 - \int_0^{\theta_i} f_M(\theta')\, 2\pi\, \theta'\, d\theta' \tag{28}$$

since $\int_0^\infty f_M(\theta')\, 2\pi\, \theta'\, d\theta'$ is normalized to 1.

The corresponding number for single Rutherford scattering only, is

$$1 - \exp\left[-n \int_{\Omega_i}^{4\pi} \left(\frac{d\sigma}{d\Omega}\right)_C d\Omega\right] . \tag{29}$$

Since the Molière correction includes single Rutherford scattering (no form factor is considered), the multiple Coulomb scattering correction $\kappa(\Omega,n)$ in Eq. (12) becomes the difference between Molière and single Rutherford scattering correction:

$$\kappa(\Omega, n) = \frac{1}{n}\left|\ln \int_0^{\theta(\Omega)} f_M(\theta')\, 2\pi\, \theta'\, d\theta'\right| - \int_\Omega^{4\pi} \left(\frac{d\sigma}{d\Omega}\right)_C d\Omega$$

$$\simeq \frac{1}{n} \int_{\theta(\Omega)}^{\infty} f_M(\theta')\, 2\pi\, \theta'\, d\theta' - \int_\Omega^{4\pi} \left(\frac{d\sigma}{d\Omega}\right)_C d\Omega \quad \text{for } \theta \gg \chi_c . \tag{30}$$

4.1.3 Additional corrections

For very small scattering angles $|t| \leq 0.002$ (GeV/c)^2, partial cross-sections are sensitive to

i) the finite size (3 cm Ø) and the mean divergence (≃ 6 mrad) of the incoming beam; and
ii) the scattering of protons by the electrons of the atom.

Both effects cause bigger Coulomb corrections, and were estimated by calculating a slightly higher effective Molière parameter $B' > B$, according to Cormack[14] for the beam and Fano[15,12] for the electron scattering.

Figure 10 illustrates, as an example, all Coulomb corrections for p-^{4}He partial cross-sections in a 75 cm long target, and confirms that data below $|t| = 0.001$ (GeV/c)^2 cannot be used because the Coulomb corrections and their uncertainties rise very quickly.

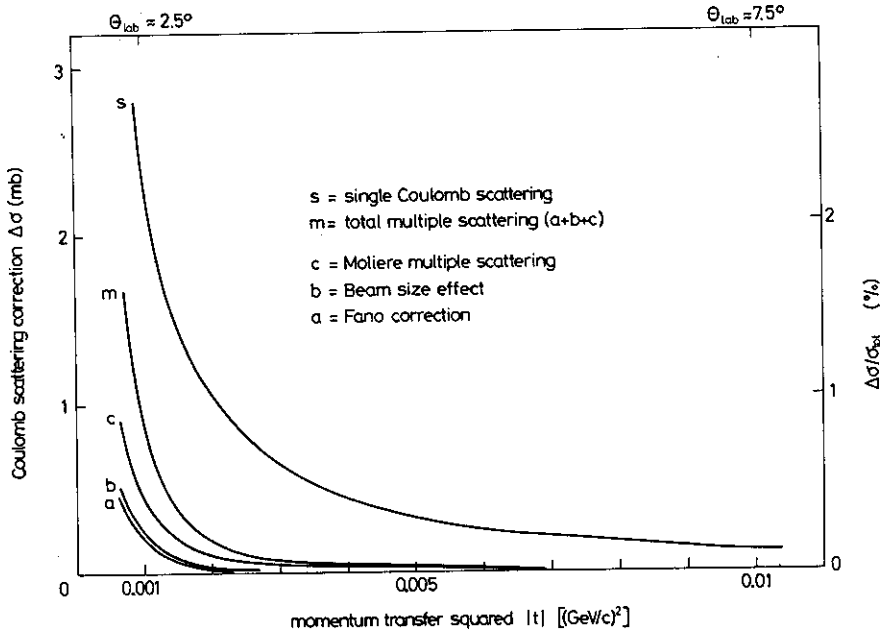

Fig. 10 Coulomb scattering corrections for p-^{4}He data at 273 MeV

4.2 Coulomb-nuclear interference correction and extrapolation

In Section 2.3 we have explained qualitatively the possibility of extracting the real part of the nuclear forward scattering amplitude from partial cross-sections in the Coulomb-nuclear interference region.

Denoting by α the ratio of real to imaginary part of the forward scattering amplitude f, and using the optical theorem which relates the imaginary part to the total cross-section, the dominant term in the interference cross-section becomes

$$\mathrm{Re}\, f_C \cdot \mathrm{Re}\, f \sim \frac{\alpha\, \sigma_{tot}\, Z}{t} \quad . \tag{31}$$

The Z-dependence tells us that any structure in Coulomb-corrected partial cross-sections [Fig. 3, Eq. (16)] is easier to detect in heavier elements. Since the precision of the partial cross-sections in this experiment is limited to about 0.3% owing to statistics and systematic uncertainties in the apparatus, Re f could be extracted only from the ^{4}He, ^{12}C, and ^{16}O data. This method failed in ^{1}H and ^{2}D. We have therefore calculated the interference correction in Eq. (12), using the most recent nucleon-nucleon Livermore phase-shift analysis[1] to get the forward scattering amplitudes.

4.2.1 Evaluation of the pp data

Assuming isotopic spin invariance in the nucleon-nucleon interaction, the (pp) and (nn) systems are pure isospin triplet states (I = 1) and are isosymmetric:

$$I_3(\mathrm{pp}) = +1$$

$$I_3(\mathrm{nn}) = -1 \quad .$$

Therefore the scattering in both systems is described by the same strong interaction amplitudes.

The direct product of the individual spin spaces of each nucleon reduces into a singlet and triplet subspace

$$\tfrac{1}{2} \otimes \tfrac{1}{2} = 0 \oplus 1 \quad ,$$

with total spin S = 0 and S = 1, respectively.

The scattering matrix M in terms of helicity amplitudes $f_{\mu_i \mu_f}$ has the form[16]

$$M = \left(\begin{array}{c|ccc} f_s & \multicolumn{3}{c}{0} \\ \hline & f_{11} & f_{10} & f_{1-1} \\ 0 & f_{01} & f_{00} & f_{0-1} \\ & f_{-11} & f_{-10} & f_{-1-1} \end{array}\right) ; \tag{32}$$

$\mu_{i,f} = \lambda_1 - \lambda_2$ denote total helicities of the initial and final states of the system, and $\lambda_{1,2}$ are the helicities of each individual nucleon in the direction of its propagation.

As an example we illustrate the single spin-flip amplitude f_{10}:

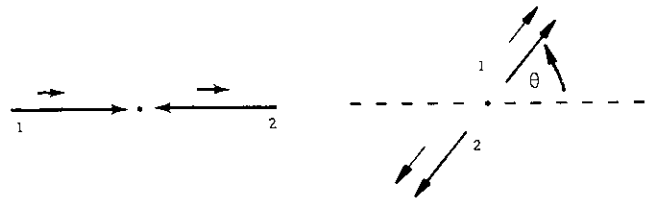

Table 4

	Initial state	Final state
λ_1	$+\frac{1}{2}$	$+\frac{1}{2}$
λ_2	$-\frac{1}{2}$	$+\frac{1}{2}$
μ	+1	0

By space reflexion and time reversal invariance, the following symmetries are valid:

$$f_{11} = f_{-1-1}\,, \quad f_{1-1} = f_{-11}\,, \quad f_{10} = f_{0-1} = -f_{01} = -f_{-10}\,.$$

Therefore, M has only five independent amplitudes: three non-flip amplitudes f_s, f_{11}, f_{00}; one single-flip amplitude f_{10}; and one double-flip amplitude f_{1-1}.

The averaged non-flip amplitude, i.e. the spin-independent amplitude of the system equals the trace of M:

$$f = \tfrac{1}{4}(f_s + f_{00} + 2f_{11})\,. \tag{33}$$

This amplitude was calculated in the Coulomb-nuclear interference region for the nn system (I = 1) by applying the partial wave decomposition of the helicity amplitudes[16] to the most recent energy dependent phase-shift analysis X of the Livermore group[1]. The amplitude f alone interferes with the Coulomb amplitude, which results in an interference cross-section:

$$\left(\frac{d\sigma}{d\Omega}\right)_{Cni}(pp) = 2\ \mathrm{Re}\,(f \cdot f_C^*)\,, \tag{34}$$

where f_C, the Coulomb amplitude, is given by

$$f_C = - \frac{\eta_C}{2k \sin^2 \frac{\theta}{2}} e^{-i\delta} \quad ,$$

where (35)

$$\eta_C = \frac{Z}{\beta} \left(\frac{e^2}{\hbar c}\right) \quad Z = 1$$

$$\delta = \eta_C \ln \sin^2 \frac{\theta}{2}$$

$$k = \text{c.m. momentum} \ .$$

The phase δ [17-18] stands for the phase difference between the pure Coulomb amplitude and the phase shift of the nuclear amplitude due to radiative corrections. It is based on a point charge Coulomb potential, and is a good approximation for small angles, particularly in the interference region if the form factors stay very close to one.

Figure 11 shows the interference cross-sections as function of $|t|$ for several kinetic energies of the incoming proton. It is mainly negative as the interference is destructive

$$\left[\alpha = \frac{\text{Re } f}{\text{Im } f} (0°) > 0 \right] .$$

The quoted energy-dependent analysis[1] consists of a unique set of phase shifts and is reliable up to 450 MeV. Nevertheless, the phases were extrapolated to 550 MeV, hoping

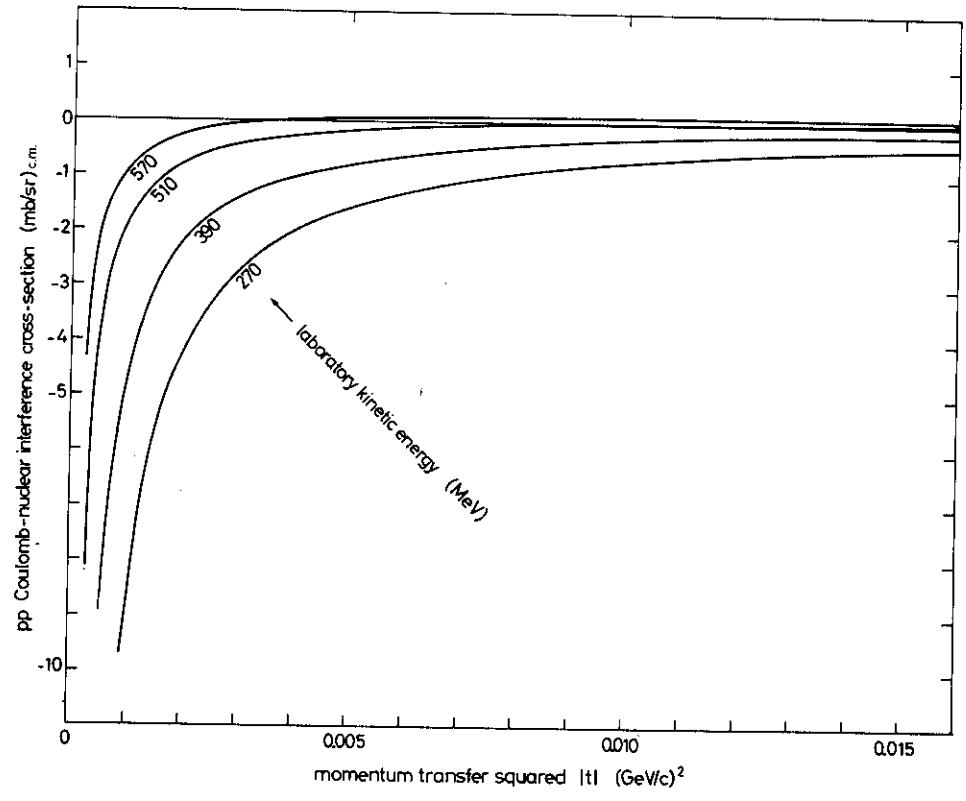

Fig. 11 pp Coulomb-nuclear interference differential cross-sections obtained from phase shifts

to get at least a rough estimate of the correction, which, in any case, turned out to be very small since Re f (0^0) reaches zero and changes sign in this energy region.

All partial cross-sections have been corrected by the interference effect, the integral of Eq. (34), and then fitted with a straight line in order to extrapolate to the total cross-section at zero solid angle.

Figure 12 illustrates, as an example, the data at 268 MeV (data for three different positions of the transmission counters have been measured). We see that at low energies the interference correction and the Coulomb scattering correction are very important and considerably larger than the statistical errors of the experimental data. Thus the error one quotes for the total cross-section is strongly influenced by the confidence one has in the manner in which these corrections are made.

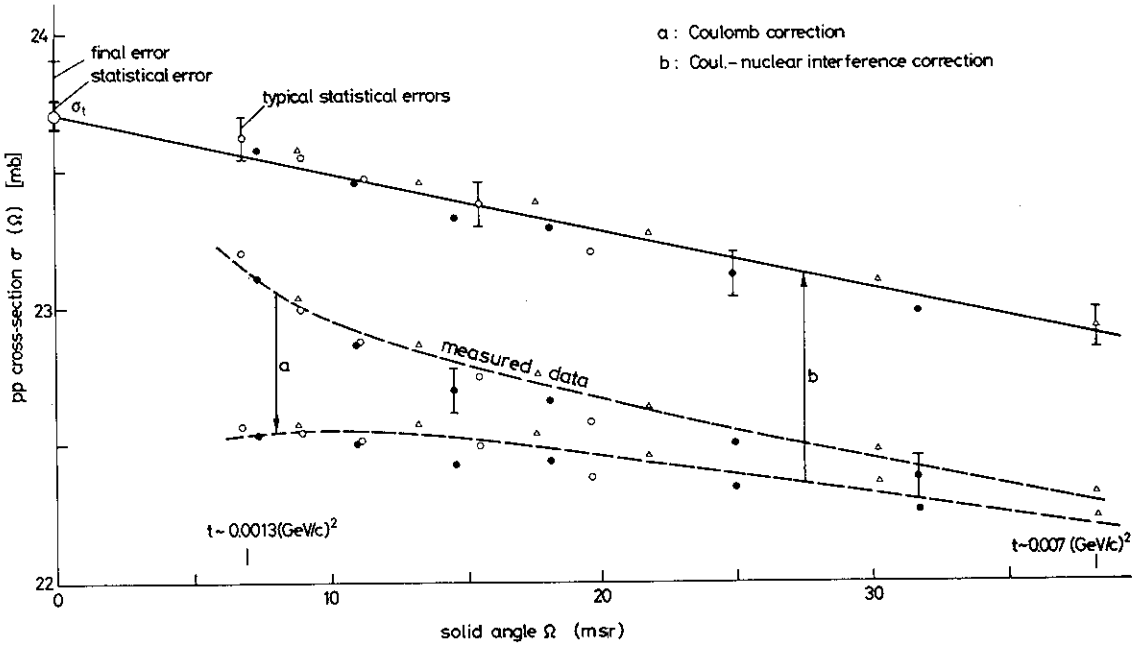

Fig. 12 Extrapolation for σ_{tot}(pp) at 268 MeV

4.2.2 Evaluation of the pd data

The nuclear scattering of a proton on a deuteron can be described to a good approximation with multiple scattering theory, provided that the energy of the incident proton is high enough, i.e. the de Broglie wavelength λ is small against the r.m.s. radius R of the deuteron. This condition is still satisfied in our energy region.

$$\lambda \simeq 0.2 \text{ fermi} \ll R \simeq 2.8 \text{ fermi} .$$

In the very small angle scattering limit, the incident proton has a large impact parameter and therefore essentially scatters from one nucleon only. According to the impulse-approximation, the spin-independent single scattering pd amplitude is the coherent sum of

the Coulomb amplitude f_C and the spin-independent proton-proton and proton-neutron amplitudes f_{pp} and f_{pn}:

$$f_{pd}^{C} = (f_C + f_{pp} + f_{pn}) \cdot F(t) \ , \tag{36}$$

where F(t) is the deuteron form factor, which is assumed to be equal for f_C and f_{pp} (f_{pn}), and which drops very fast with increasing $|t|$ because of the weak binding and the relatively large distance between the two nucleons in the deuteron.

In this approach f_C interferes with

$$f_{pd} = f_{pp} + f_{pn} \ , \tag{37}$$

resulting in an interference cross-section

$$\left(\frac{d\sigma}{d\Omega}\right)_{Cni} (pd) = 2 \ Re \ (f_C \cdot f_{pd}^{*}) \cdot F^2 \ . \tag{38}$$

The amplitude f_{pn} also was obtained from phase shifts, as was f_{pp} in Section 4.2.1, although pn phase shifts are much less reliable owing to the po . pn experimental data.

The calculated interference cross-sections (38) were compared to the Coulomb-nuclear interference of experimental pd differential cross-section data at 146 and 325 MeV. This test confirmed that the calculated cross-sections had the right order of magnitude; hence it gave us confidence in the applied interference correction, especially at low energies where it is important.

The interference corrections [the integral of Eq. (38)]

$$\Delta\sigma_{Cni} = - \int_{\Omega}^{4\pi} \left(\frac{d\sigma}{d\Omega}\right)_{Cni} d\Omega \tag{39}$$

added to all partial cross-sections are plotted in Fig. 13 for several energies. Total cross-sections suffered a correction of less than 1%.

The order of magnitude of the interference correction is dictated by α, the ratio of the real to the imaginary part of the spin-independent forward scattering amplitudes f_{pp} and f_{pn}, respectively [see Eq. (31)]. Figure 14 compares α_{pp} and α_{pn} as obtained from phase shifts[1] with forward dispersion relation predictions[19-20] and experiments[21].

Large discrepancies show up in the few hundred MeV region, and no direct precise experimental data is available for the moment. This uncertainty leads to considerable errors in total cross-sections, as discussed in Section 4.3.

4.2.3 Evaluation of p-^{4}He, ^{12}C, and ^{16}O data

In all these elements the Coulomb-nuclear interference cross-section is big enough to contribute to a measurable curvature at small angles for partial cross-sections $\sigma_{corr}(t)$ as a function of t [σ_{corr} are the measured partial cross-sections corrected by pure Coulomb scattering, cf. Eq. (16) and Fig. 3]. In order to analyse the data, we approximated the differential cross-sections on the right-hand side of Eq. (12) in the following phenomenological way.

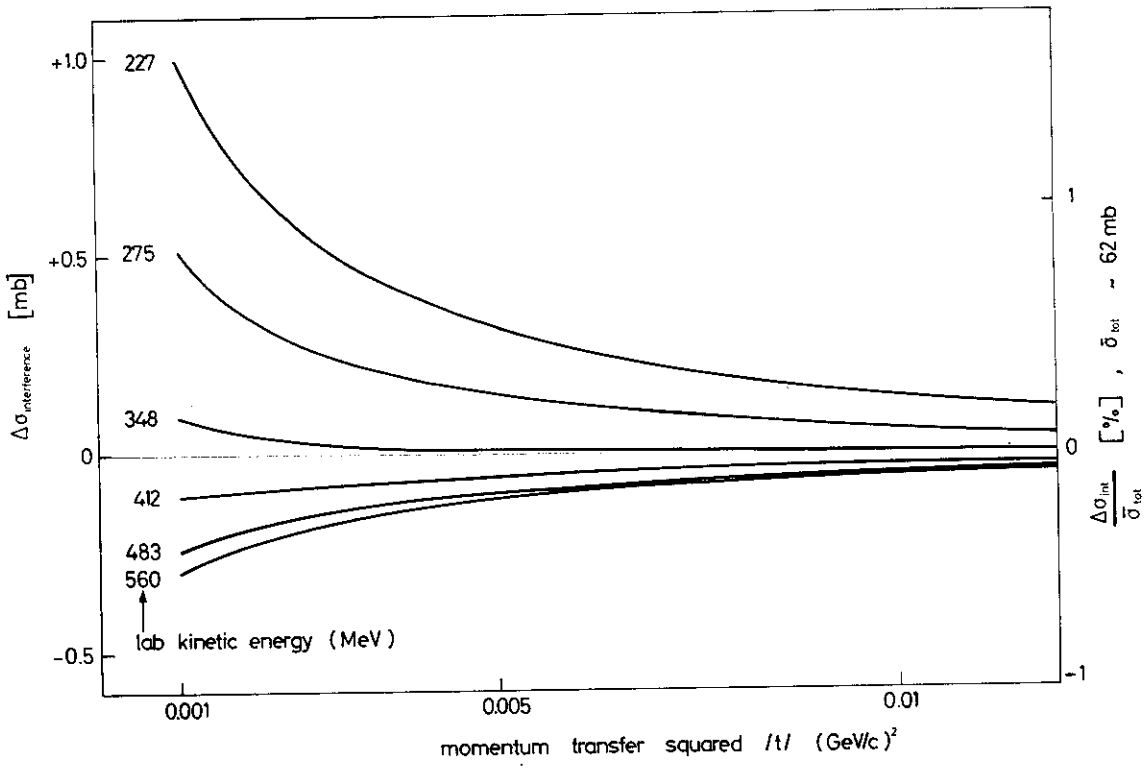

Fig. 13 Coulomb-nuclear interference corrections for pd data

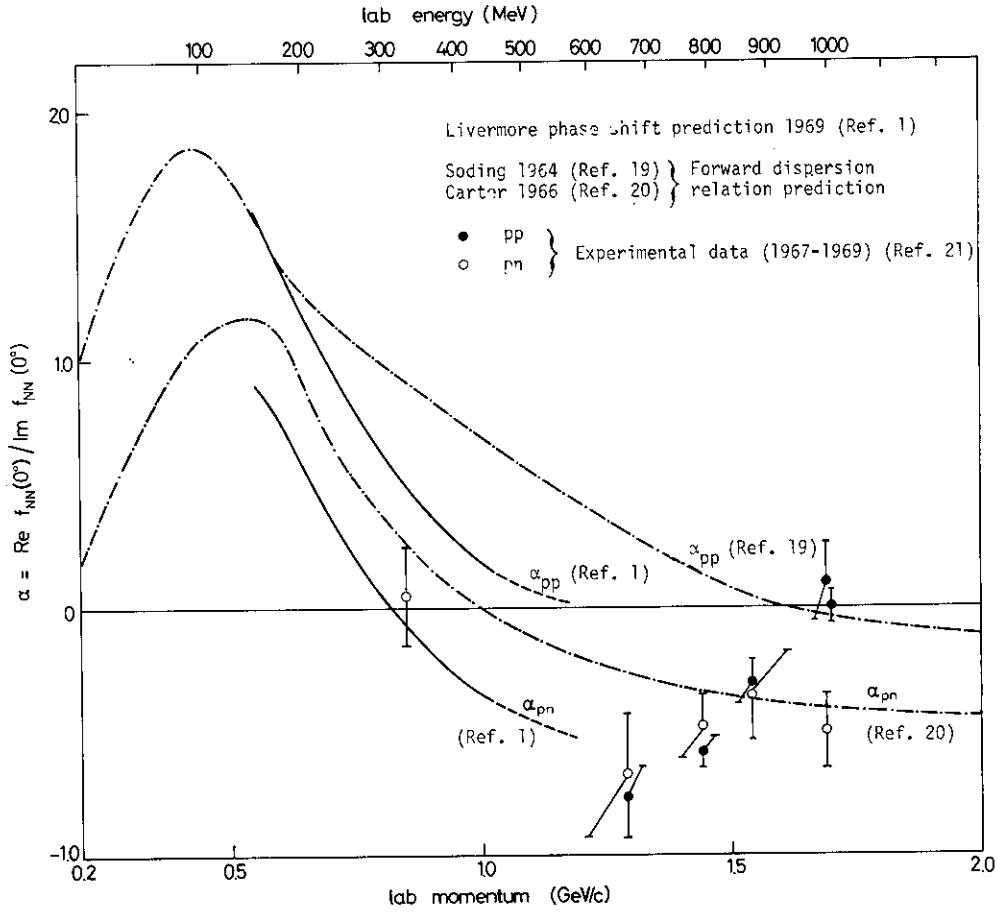

Fig. 14 Ratio of the real to the imaginary part of the spin-independent forward scattering nucleon-nucleon amplitudes

a) Nuclear elastic scattering

The elastic scattering matrix M for a proton to be scattered on an isospin and spin zero nucleus is of the form

$$M = f \cdot \mathbf{1} + g \cdot (\vec{n} \cdot \vec{\sigma}) \ , \tag{40}$$

where f and g are spin-non-flip and spin-flip amplitudes, respectively, and $\vec{n}$ is the normal to the scattering plane.

The amplitude f was approximated at small angles by

$$f = \frac{ik}{4\pi} \sigma_{tot}(1 - i\alpha) \, e^{(\gamma^2/2)\cdot t} \tag{41}$$

using the optical theorem and assuming that Re f and Im f have the same t-dependence. The slope parameter γ^2 was taken from measured differential cross-section data in this energy region, and considered as energy-independent because it has a very small influence on the results.

Table 5

	^{4}He	^{12}C	^{16}O	
γ^2 =	27	70	84	$(GeV/c)^{-2}$

The spin-flip amplitude g is proportional to sin θ; it vanishes in the forward direction and stays very small in our angular region. It does not interfere with the Coulomb amplitude. We have neglected its contribution to the partial cross-sections.

b) Inelastic scattering

There exist only few experimental data on the distribution of secondary products at small angles; in particular, the behaviour of charged inelastic products in our transmission counters is unknown. However, we believe that the order of magnitude *and* the t-dependence of $(d\sigma/d\Omega)_{inel}$ in Eq. (12) do not compete with the interference cross-section [which is as large as the nuclear elastic cross-section for $|t| \simeq 0.004$ $(GeV/c)^2$ and varies as $1/t$]. Therefore we simply assume that $(d\sigma/d\Omega)_{inel} = C_{inel}$ is a constant in the small angular range in which data were measured.

c) Coulomb scattering

The Coulomb amplitude f_C has already been given in Eq. (35):

$$f_C = - \frac{\eta_C}{2k \sin^2 \frac{\theta}{2}} \, e^{-i\delta_B} \cdot F(t) \ . \tag{42}$$

However, we have now included the form factor F(t) defined in Section 4.1.1 and used a Coulomb phase difference δ_B which was derived by Bethe[18] allowing for a screened Coulomb potential for small impact parameters $b \lesssim R$:

$$\delta_B = -2\eta_C \ln \frac{1.06}{ka\theta} \quad , \tag{43}$$

where

$$a = \sqrt{\frac{2}{3}}\, R \quad .$$

The fact that δ_B differs considerably from the phase derived by Solov'ev[17] [Eq. (35)] is irrelevant in this analysis, as the contribution Im f · Im f_C to the interference cross-section is very small and is only comparable to Re f · Re f_C for $\alpha < 0.02$.

The amplitudes and cross-sections in a, b, and c inserted into Eq. (12) lead to partial cross-sections as a function of Ω, of the form:

$$\sigma^{th}_{corr}(\Omega) = \sigma_{tot} - \underbrace{(1+\alpha^2)\,\sigma^2_{tot}\,\omega_1(\Omega)}_{\text{nuclear elastic}} - \underbrace{C_{inel}\cdot\Omega}_{\text{inelastic}} - \underbrace{\alpha\,\sigma_{tot}\,\omega_2(\Omega) - \sigma_{tot}\,\omega_3(\Omega)}_{\substack{\text{Coulomb-nuclear}\\ \text{interference}}} \quad , \tag{44}$$

where

$$\omega_1(\Omega) = \frac{\left(1 - e^{\gamma^2 t(\Omega)}\right)}{16 \cdot \pi \cdot 10 \cdot 0.1973^2\ \gamma^2} \quad ,$$

$$\left.\begin{matrix}\omega_2(\Omega)\\ \omega_3(\Omega)\end{matrix}\right\} = \frac{Z}{137.036 \cdot \beta} \int_{t(\Omega)}^{t_{max}} \frac{e^{(\gamma^2/2)\cdot t}\, F(t)}{t} \left\{\begin{matrix}\cos\delta_B\\ \sin\delta_B\end{matrix}\right\} dt \quad .$$

The three unknown parameters σ_{tot}, α, and C_{inel} were obtained by fitting this function to the measured cross-sections $\sigma^{exp}_{corr}(\Omega_i)$, i = 1, ..., N, N > 12 in general, using the method of least squares:

$$\chi^2 = \sum_{i=1}^{N} \left[\sigma^{th}_{corr}(\Omega_i) - \sigma^{exp}_{corr}(\Omega_i)\right]^2 = \underline{\min} \quad . \tag{45}$$

In first approximation the best fitted values $\bar{\sigma}_{tot}$, $\bar{\alpha}$, $\bar{C}_{inel}$ do not depend on correlations between measured partial cross-section data. However, final data were computed taking correlations into account as described in Section 4.3.1.

Figure 15 illustrates the order of magnitude and the Ω- or t-dependence of the terms in Eq. (44) for p-^{4}He data at 273 MeV for best fitted parameters

$$\begin{aligned}\sigma_{tot} &= 105.4 \text{ mb}\\ \alpha &= 0.52\\ C_{inel} &= 32 \text{ mb/sr} \quad .\end{aligned}$$

Note that the nuclear elastic term (II) stays linear in |t| up to |t| ≈ 0.005 (GeV/c)^2.

Oxygen data have been measured in a water target. The necessary input data $\sigma^{exp}_{corr}(^{16}O)$ for the fit were obtained by

$$\sigma^{^{16}O}_{corr}(\Omega) = \sigma^{H_2O}_{corr}(\Omega) - 2\,\sigma^{H}_{corr}(\Omega) \quad , \tag{46}$$

where $\sigma^{H}_{corr}(\Omega)$ were taken from the experimental hydrogen data (Section 4.2.1.).

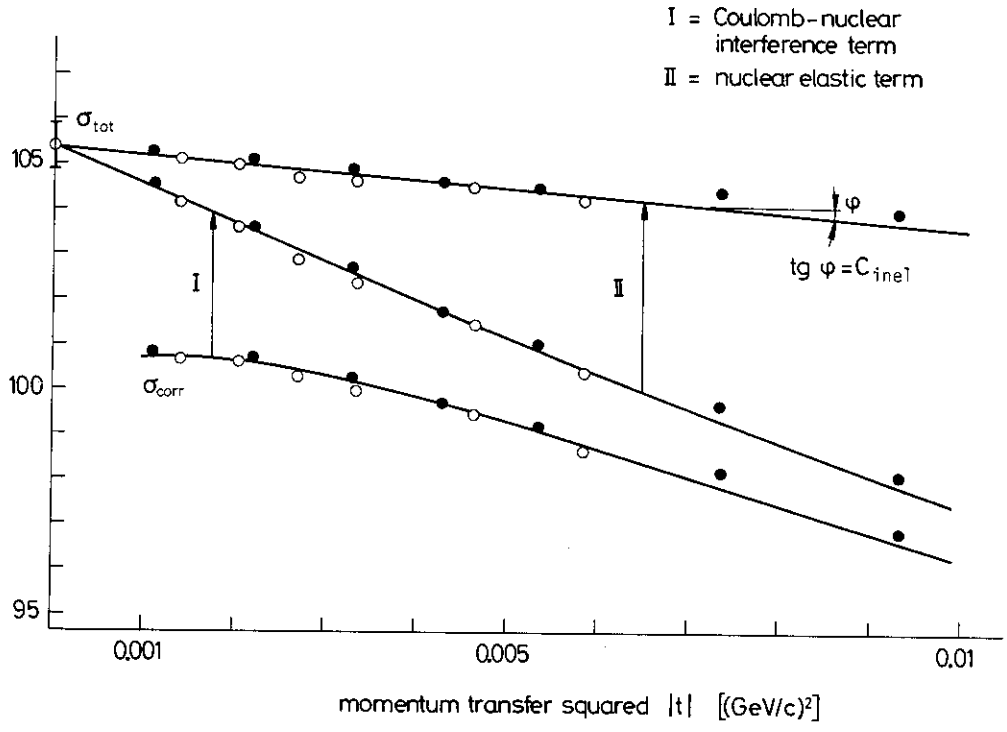

Fig. 15 Extrapolation for $\sigma_{tot}(p-^4He)$ at 273 MeV

4.3 Error estimates

4.3.1 Random errors

In this section we list the errors which are random and independent between data at different energies.

i) Counting statistics: All total cross-sections have been measured with ±0.2% statistical accuracy.

ii) Stability of efficiencies: The efficiencies of the transmission counters were measured regularly and stayed extremely stable; no shift was observed during the data-taking time:

$$\frac{\Delta\sigma_{tot}}{\sigma_{tot}} \leq \pm 0.05\% \ .$$

iii) Accidentals: We attributed a random error, due to accidental coincidences, of half the biggest correction in Section 3.4, i.e.

$$\frac{\Delta\sigma_{tot}}{\sigma_{tot}} = \pm 0.1\% \ .$$

iv) Background: For liquid targets, a small correction for different absorptions of the dummy target compared to the empty target was applied (Section 3.2). Again we estimated the error on this correction to be half of the correction, i.e.

$$\frac{\Delta\sigma_{tot}}{\sigma_{tot}} = \pm 0.15\% \ .$$

Since "target out" transmission measurements were energy sensitive, partial cross-sections have been systematically corrected (Section 3.6). We believe that any error from this effect did not exceed ±0.1% in the total cross-section, but may affect α if the true correction is not linear in Ω.

v) Data analysis: In the data analysis of He, C, and O, random errors for the three fitted parameters $\bar{\sigma}_{tot}$, $\bar{\alpha}$, $\bar{C}_{inel}$ were obtained by computing the log likelihood function L and projecting the three-dimensional volume

$$L(\sigma_{tot}, \alpha, C_{inel}) = -\tfrac{1}{2}\chi_3^2 = \text{constant} \tag{47}$$

on the axes σ_{tot}, α, C_{inel}.

The quantity -2L has a χ_3^2 distribution provided σ_{tot}, α, and C_{inel} are Gaussian distributed around their true values, and L is normalized such that $L_{max} = L(\bar{\sigma}_{tot}, \bar{\alpha}, \bar{C}_{inel}) = 0$. We have chosen a probability content $P(\chi_3^2 \leq 2L) = 70\%$; therefore $\chi_3^2 = 3.6$ and $L = -1.8$. At a given energy all partial cross-sections have been measured in u sets of seven data points each ($u \geq 2$), corresponding to u different distances between target centre and transmission counter array. The data in each set are very strongly correlated, because they have been measured simultaneously with the same incoming protons. The correlation matrix m_7 has been obtained by repeating a transmission experiment six times at a fixed energy and geometry, and computing the correlation coefficients from these data:

$$m_7 = \begin{vmatrix} 1 & 0.99 & 0.98 & 0.97 & 0.96 & 0.93 & 0.91 \\ 0.99 & 1 & 0.98 & 0.97 & 0.95 & 0.92 & 0.90 \\ 0.98 & 0.98 & 1 & 0.99 & 0.98 & 0.93 & 0.93 \\ 0.97 & 0.97 & 0.99 & 1 & 0.99 & 0.95 & 0.95 \\ 0.96 & 0.95 & 0.98 & 0.99 & 1 & 0.97 & 0.95 \\ 0.93 & 0.92 & 0.93 & 0.95 & 0.97 & 1 & 0.98 \\ 0.91 & 0.90 & 0.93 & 0.95 & 0.95 & 0.98 & 1 \end{vmatrix} \tag{48}$$

Denoting by $\vec{\Delta}$ the vector

$$\vec{\Delta} = \left\{\left[\sigma_{corr}^{exp}(\Omega_1) - \sigma_{corr}^{th}(\Omega_1)\right], \ldots, \left[\sigma_{corr}^{exp}(\Omega_{7u}) - \sigma_{corr}^{th}(\Omega_{7u})\right]\right\},$$

where σ_{corr}^{exp} and σ_{corr}^{th} represent the partial cross-sections defined in Eqs. (44) and (45), the log likelihood function is given by

$$L = -\frac{1}{2}\frac{1}{\nu^2}\left(\chi^2 - \chi^2_{min}\right), \tag{49}$$

where

$$\chi^2 = \left(\vec{\Delta}\, m^{-1}\, \vec{\Delta}^{+}\right),$$

and

$$m = \begin{vmatrix} m_7 & & 0 \\ & m_7 & \\ & & \ddots \\ 0 & & m_7 \end{vmatrix} \Bigg\} 7 \cdot u .$$

The errors v of all partial cross-sections are assumed to be about equal and only known by the order of magnitude

$$0.2\% < \frac{v}{\sigma_{exp}} < 1\% \quad .$$

Therefore v^2 was calculated from the data

$$v^2 \simeq \frac{\chi^2_{min}}{\nu} \tag{50}$$

where $\nu = 7u - 3$ is the degree of freedom of the fit. If v^2 was found within the above interval, the fit was considered to be reasonable.

The errors of the best fitted parameters are given by the following orders of magnitude:

$$\frac{\Delta\sigma_{tot}}{\sigma_{tot}} = \pm(1 - 3)\% \; ; \quad \Delta\alpha = \pm(0.1 - 0.15) \; ; \quad \frac{\Delta C_{inel}}{C_{inel}} = \pm(20 - 40)\% \; .$$

They dominate all the errors previously mentioned.

vi) Range-energy measurement: The peak position of the differential range curve can be located experimentally within ±2 MeV (cf. Section 3.7). This error was converted into errors in total cross-sections and α's being for most cases negligible. All random errors have been added quadratically and are listed in the tables of Section 5.

4.3.2 Systematic errors

We subdivided systematic errors into two classes: those which may move all data as a function of energy systematically up or down, and those which influence results in one direction only.

a) Systematic errors of both signs

i) Target length and density: These errors are already listed in Table 2, Section 3.2.
ii) Errors on the Coulomb correction in pp and pd total cross sections: We attributed a 10% uncertainty to the single and multiple Coulomb scattering correction.

Table 6

	$\pm \Delta\sigma_{tot}/\sigma_{tot}$	
lab. energy	pp	pd
200 MeV	0.3%	0.1%
550 MeV	0.05%	0.02%

iii) Errors in the Coulomb-nuclear interference correction for pp and pd data: The large discrepancies in $\alpha = \mathrm{Re}\, f_{NN}/\mathrm{Im}\, f_{NN}$ (0°) illustrated in Fig. 14 force us to accept big errors on the interference correction.

We assumed $\Delta\alpha_{pp} \simeq \pm 0.2$, which propagates into systematic errors in the pp total cross-sections of about ±0.8%, thus dominating all other errors. For the case of α_{pn} the situation is even worse, since the (I = 0) phase-shift analysis is not unique. Signell and Holdeman[22] mention a serious ambiguity in the phase parameters near 330 MeV. However, an error as large as ±0.4 in α_{pd}, the real over the imaginary part of the nuclear pd amplitude ($f_{pd} = f_{pp} + f_{pn}$), affects the total pd cross-section by ±0.9% only.

iv) Systematic errors in the He, C, O data analysis: The analytic function Eq. (44), fitted to the partial cross-sections, depends on various constants which are subject to an error.

- kinetic energy E	$\Delta E = \pm 2$ MeV
- r.m.s. radius R of the nucleus	$\Delta R/R = \pm 10\%$
- slope parameter γ^2 of the nuclear differential cross-sections	$\Delta\gamma^2/\gamma^2 = \pm 20\%$.

Furthermore, the partial cross-sections $\sigma_{corr}^{exp}(\Omega)$ may be systematically in error owing to uncertainties in the single and multiple Coulomb scattering corrections; again we assumed a 10% error in this correction. Each error propagates separately into systematic errors of the best fitted parameters σ_{tot}, α, and C_{inel}. We have added them all quadratically and obtained the following orders of magnitude:

$$\Delta\sigma_{tot}/\sigma_{tot} = \pm 0.6\%$$

$$\Delta\alpha = \begin{cases} \pm 0.13 \text{ at } 200 \text{ MeV} \\ \pm 0.07 \text{ at } 550 \text{ MeV} \end{cases}$$

$$\Delta C_{inel}/C_{inel} = \pm 15\% \ .$$

b) Systematic errors in one direction

i) Range curves: Range curves in comparison with floating wire experiments provided systematically smaller beam energies (2 to 3 MeV). This discrepancy falls within errors of range-energy conversion tables.

ii) Effective efficiency: We estimated that any change of effective efficiency (defined in Section 2.1) would decrease total cross-sections by 0.1% at most.

iii) Density of liquid hydrogen: The conversion of vapour pressure into density was based on the assumption that all liquid H_2 was in the para state. A 20% ortho H_2 contamination would decrease total cross-sections by 0.05% only.

All systematic errors (added quadratically) are considered to influence the scale in the plots of Section 5 and are not included in the quoted errors in the tables.

5. RESULTS AND DISCUSSION

5.1 Results

In the following tables (7 to 11) and figures (16 to 21) we present our results for the proton total cross-sections of H, D, He, C, and O together with the ratio of the real to the imaginary part of the proton-nucleus forward scattering amplitude.

Previous experimental data in the figures are taken from various compilations[23-26].

In Fig. 17 [σ_{tot}(pd)] we have included only the most recent experimental data because they extend over larger energy ranges.

In the figures of the carbon and oxygen total cross-sections we distinguish simply between the proton and neutron experiments in order to get an impression of the validity of charge symmetry.

The data and curves are discussed in Section 5.2.

The forward amplitude f on an isospin zero target with A nucleons is related by the impulse approximation to the isospin averaged nucleon-nucleon amplitude (later referred to by f_{NN}) by:

$$f = A \cdot f_{NN} = A\tfrac{1}{2}(f_{pp} + f_{pn}) \quad , \tag{51}$$

where f_{pp} and f_{pn} are the spin-independent pp and pn forward scattering amplitudes (see also Section 5.2.2). The ratio α = Re f/Im f is therefore independent of the target and should be equal to α_{NN}. Figure 21 shows that our values of α for He, C, and O agree with each other within errors in the energy range 250 to 560 MeV, but disagree with α_{NN} obtained by the Livermore phase-shift analysis[1] above 300 MeV. Below 250 MeV our data have rather large errors due to the increased difficulty of applying the multiple Coulomb scattering correction in the partial cross-sections.

Since α is the important parameter in the Coulomb-nuclear interference correction, we performed a second analysis of the partial cross-sections assuming that α as a function of energy E is known by the "smoothed" curve in Fig. 21. Below 250 MeV we believe that the phase-shift prediction for α is more reliable than any mean of our measured data. We forced the "smoothed" curve α(E) to join α_{NN}(E) from phase shifts at about 220 MeV. The "smoothed" values α and the total cross-section results of this second analysis are given in columns 6 and 7, respectively, of Tables 9, 10, and 11. These total cross-sections are plotted in the figures, since we believe that they are more reliable than those in column 3.

However our total cross-section data below 250 MeV have to be used with care. An analysis of small angle nucleon-nucleus differential cross-section and polarization data in ^{4}He and ^{12}C performed by Cromer and Palmieri[27] at 140 MeV yield for α in ^{4}He and ^{12}C the values 1.23 and 0.92 respectively. The He data agrees fairly well with the NN phase shift analysis whereas α in ^{12}C is considerably below.

Using the α-value of ^{12}C at 140 MeV as an anchor point to fix the low energy behaviour of the "smoothed" curve our p^{12}C and eventually p^{16}O total cross-sections at 151 MeV (column 7 in tables 10 and 11) would become lower by 15 mb for ^{12}C and 13 mb for ^{16}O.

Table 7

$\sigma_{tot}(pp)$

Laboratory kinetic energy (MeV)	Laboratory momentum (MeV/c)	$\sigma_{tot} \pm \Delta\sigma_{tot}$ (mb)	$\Delta\sigma_{Cni}$ a) (mb)	σ_{tot} (nn) [phase-shift analysis b)] (mb)
179.0	607	24.55 ± 0.12	+2.00	24.65
267.5	757	23.85 ± 0.10	+0.90	23.90
342.5	872	24.45 ± 0.10	+0.46	24.55
388.0	937	25.65 ± 0.10	+0.34	25.50
406.5	963	26.30 ± 0.10	+0.22	26.00
439.5	1009	27.75 ± 0.14	+0.13	27.10
502.5	1093	30.95 ± 0.15	-0.02	30.15
513.5	1108	31.65 ± 0.19	-0.03	30.80
555.0	1162	34.50 ± 0.24	-0.08	33.60
		Systematic errors ± 0.8%		

a) Interference correction = difference between the quoted values of σ_{tot} and values obtained when no Coulomb-nuclear interference correction is made before extrapolation.

b) M.H. MacGregor, R.A. Arndt and R.M. Wright, Phys. Rev. 182, 1714 (1969).

Table 8

$\sigma_{tot}(pd)$

Laboratory kinetic energy (MeV)	Laboratory momentum (MeV/c)	$\sigma_{tot} \pm \Delta\sigma_{tot}$ (mb)
227	691	63.60 ± 0.5
275	769	60.75 ± 0.5
348	880	59.85 ± 0.5
412	971	61.20 ± 0.5
422	985	61.25 ± 0.5
483	1067	64.35 ± 0.5
560	1168	69.10 ± 0.5
		Systematic errors ± 1.0%

Table 9

$p-^4He$ data

Laboratory kinetic energy (MeV)	Laboratory momentum (MeV/c)	$\sigma_{tot} \pm \Delta\sigma_{tot}$ (mb)	$\alpha = \frac{Re\ f}{Im\ f} \pm \Delta\alpha$	Slope of extrapolation in lab. system $C_{inel} \pm \Delta C_{inel}$ (mb/sr)	"α" (smoothed curve)	"σ_{tot}" (mb)
224	686	106.3 ± 1.1	0.48 ± 0.14	39 ± 10	0.65	108
273	765	105.7 ± 1.1	0.52 ± 0.15	32 ± 11	0.47	105
345	875	106.8 ± 0.9	0.29 ± 0.13	49 ± 10	0.30	107
413	972	110.8 ± 1.0	0.17 ± 0.15	65 ± 20	0.20	111
430	996	112.8 ± 0.8	0.16 ± 0.13	75 ± 15	0.18	113
491	1078	117.6 ± 1.4	0.14 ± 0.22	90 ± 30	0.10	117
563	1172	123.7 ± 0.7	0.09 ± 0.10	105 ± 13	0.02	123
Systematic errors		± 0.6	± 0.10	± 10%		

Table 10

$p-^{12}C$ data

Laboratory kinetic energy (MeV)	Laboratory momentum (MeV/c)	$\sigma_{tot} \pm \Delta\sigma_{tot}$ (mb)	$\alpha = \frac{Re\ f}{Im\ f} \pm \Delta\alpha$	Slope of extrapolation in lab. system $C_{inel} \pm \Delta C_{inel}$ (mb/sr)	"α" (smoothed curve)	"σ_{tot}" (mb)
191	627	282 ± 9	$0.44 \pm {}^{0.15}_{0.18}$	-25 ± 50	0.87	307
223	684	275 ± 12	0.35 ± 0.28	$-45 \pm {}^{75}_{135}$	0.65	290
277	772	283 ± 3	0.50 ± 0.08	65 ± 20	0.46	281
306	817	288 ± 6	$0.47 \pm {}^{0.18}_{0.13}$	$100 \pm {}^{50}_{75}$	0.38	284
348	880	286 ± 6	$0.29 \pm {}^{0.18}_{0.14}$	130 ± 50	0.30	286
349	881	283.5 ± 2.5	0.21 ± 0.06	155 ± 30	0.30	286
372	914	297 ± 4	0.38 ± 0.12	$135 \pm {}^{25}_{45}$	0.26	293
392	944	300.5 ± 3.5	0.39 ± 0.10	$145 \pm {}^{35}_{45}$	0.22	295
441	1011	298 ± 5	0.11 ± 0.12	$150 \pm {}^{60}_{70}$	0.16	299
453	1027	302 ± 7	0.10 ± 0.18	$190 \pm {}^{100}_{150}$	0.14	303
456	1031	301 ± 7	0.09 ± 0.12	235 ± 45	0.14	304
467	1046	308 ± 3	0.11 ± 0.07	240 ± 35	0.13	309
497	1086	314 ± 8	$0.14 \pm {}^{0.13}_{0.10}$	315 ± 80	0.09	312
506	1098	313 ± 3	0.06 ± 0.05	301 ± 25	0.08	314
518	1113	319 ± 4	0.16 ± 0.05	335 ± 35	0.07	315
553	1159	323 ± 10	0.03 ± 0.14	380 ± 160	0.04	324
559	1167	327 ± 6	0.11 ± 0.10	380 ± 55	0.03	322
463	1041	301 ± 8 a)	0.21 ± 0.12	225 ± 50	0.13	299
502	1093	313 ± 5 a)	0.06 ± 0.05	270 ± 35	0.09	318
550	1155	323 ± 11 a)	0.00 ± 0.14	340 ± 180	0.04	324
Systematic errors		± 2	± 0.07			

a) Data measured with CH_2 target; evaluation similar to that for ^{16}O.

Table 11

$p-^{16}O$ data

Laboratory kinetic energy (MeV)	Laboratory momentum (MeV/c)	$\sigma_{tot} \pm \Delta\sigma_{tot}$ (mb)	$\alpha = \frac{Re\ f}{Im\ f} \pm \Delta\alpha$	Slope of extrapolation in lab. system $C_{inel} \pm \Delta C_{inel}$ (mb/sr)	"α" (smoothed curve)	"σ_{tot}" (mb)
190	627	$387 \begin{smallmatrix}+30\\-20\end{smallmatrix}$	0.78 ± 0.30	$-153 \begin{smallmatrix}+118\\-300\end{smallmatrix}$	0.87	394
222	682	386 ± 15	0.74 ± 0.20	$-63 \begin{smallmatrix}+100\\-180\end{smallmatrix}$	0.67	380
276	770	360 ± 6	0.50 ± 0.10	91 ± 40	0.46	357
348	880	367 ± 5	0.36 ± 0.10	148 ± 42	0.30	364
392	943	377 ± 5	0.24 ± 0.09	276 ± 56	0.23	377
442	1012	381 ± 5	0.12 ± 0.08	351 ± 70	0.16	383
516	1111	397 ± 3	0.10 ± 0.03	421 ± 21	0.07	397
558	1165	411 ± 6	0.04 ± 0.06	478 ± 60	0.03	410
Systematic errors		± 3	± 0.07			

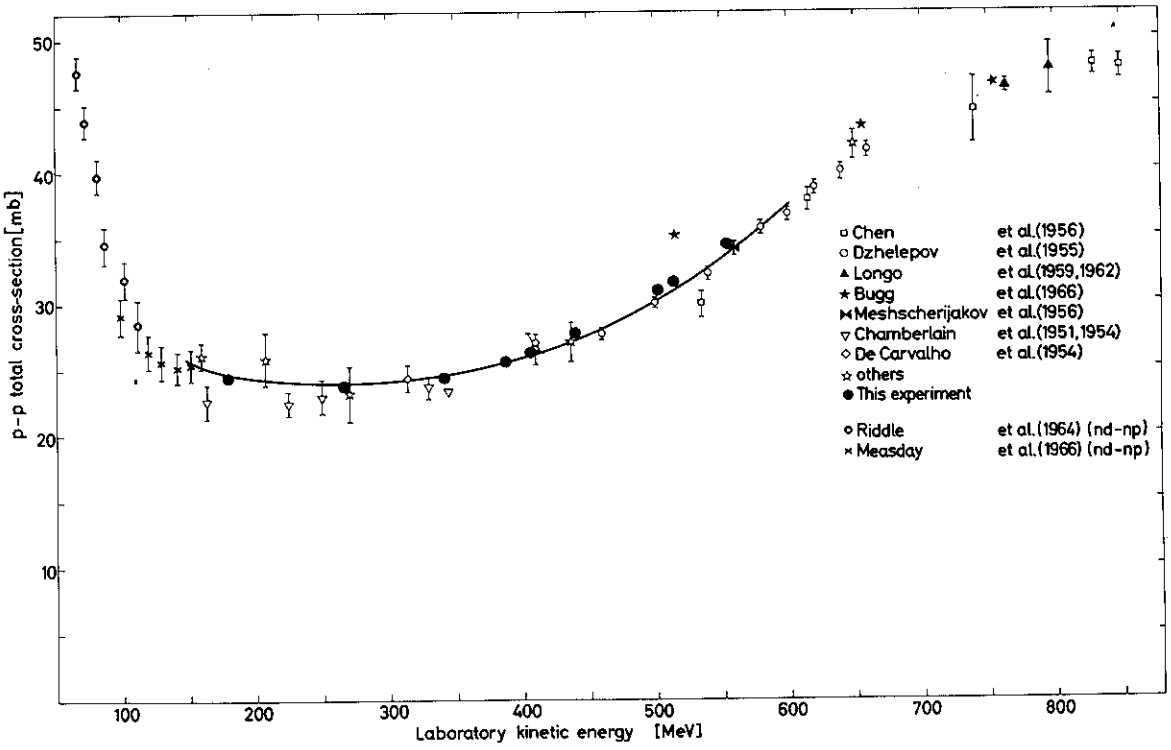

Fig. 16 p-p total cross-sections; the solid curve represents the predictions for nn total cross-sections as obtained from phase shifts (Ref. 1)

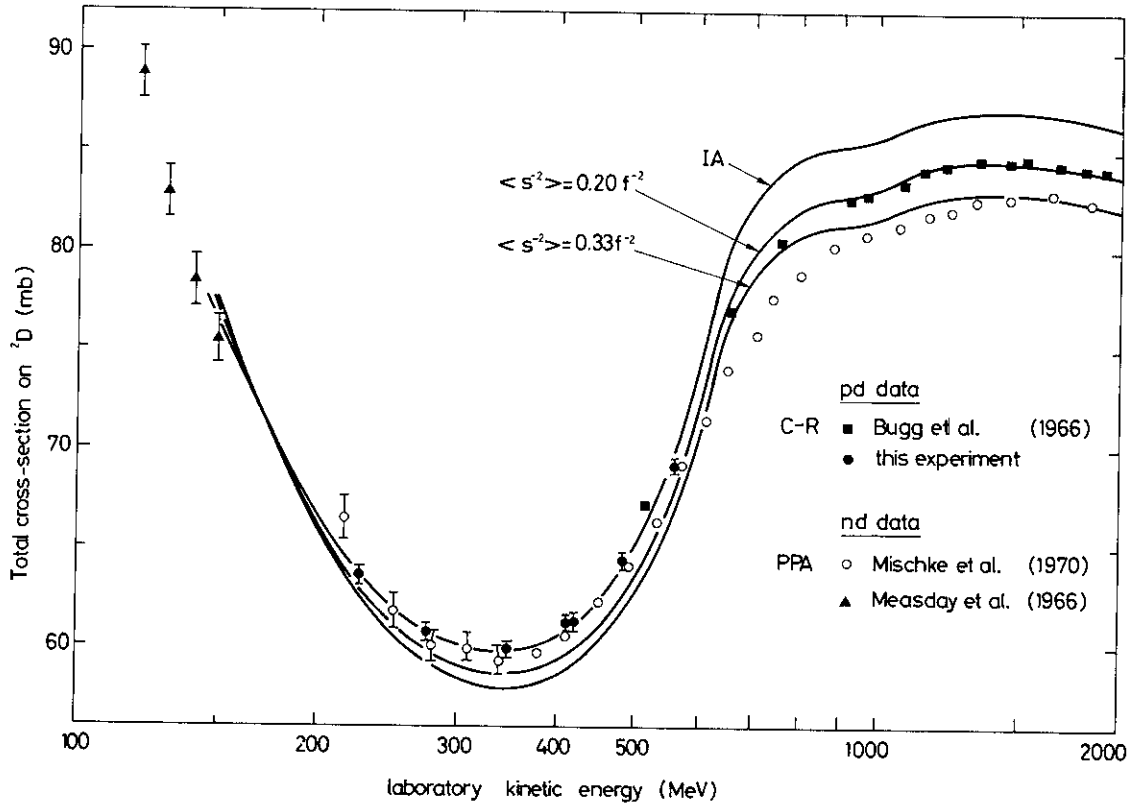

Fig. 17 Nucleon-deuteron total cross-sections; the solid curves represent Glauber model calculations.

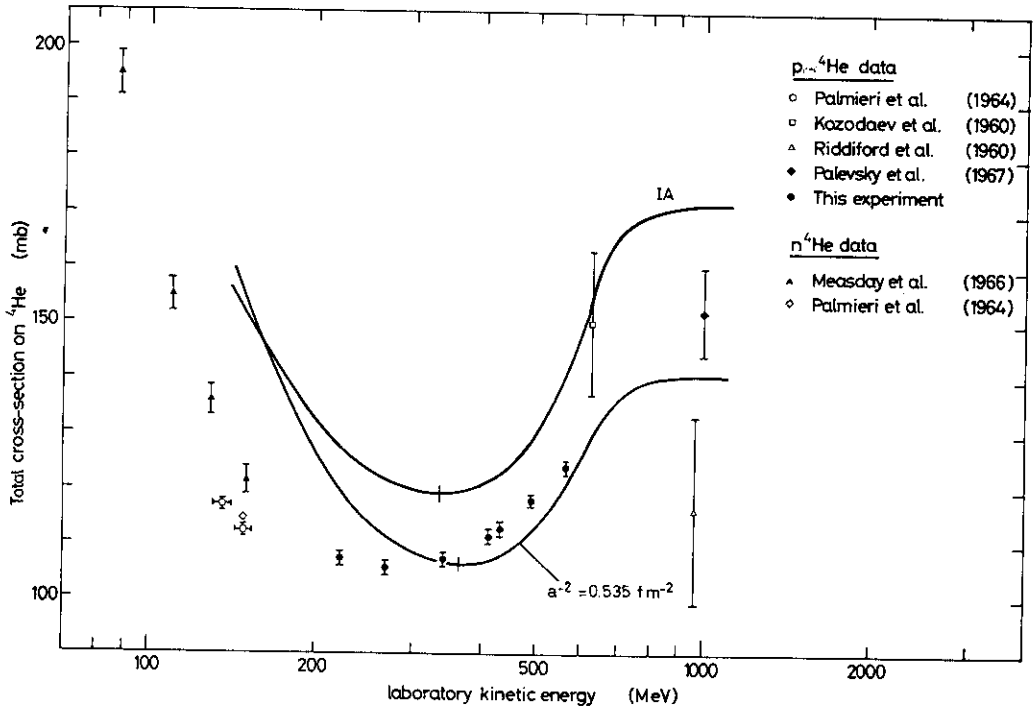

Fig. 18 Nucleon-helium total cross-sections; the solid curves represent Glauber model calculations.

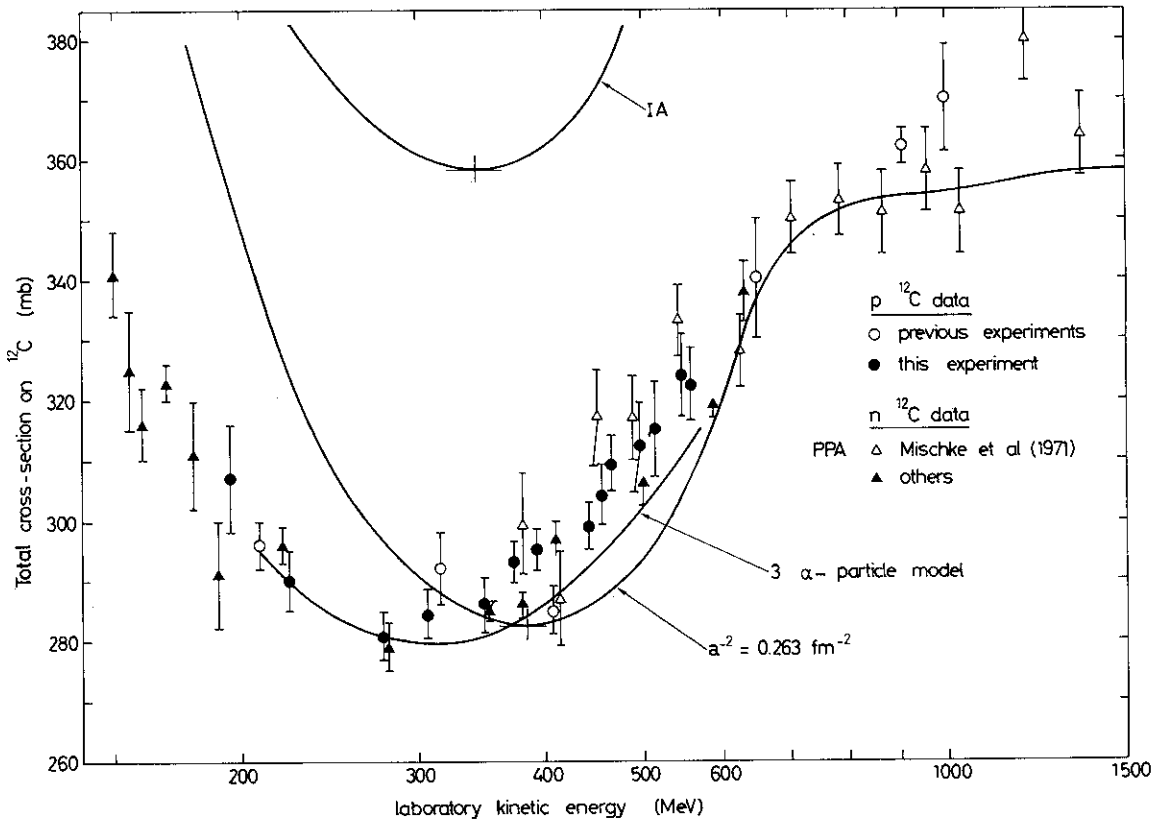

Fig. 19 Nuclear-carbon total cross-sections; the solid curves represent Glauber model calculations.

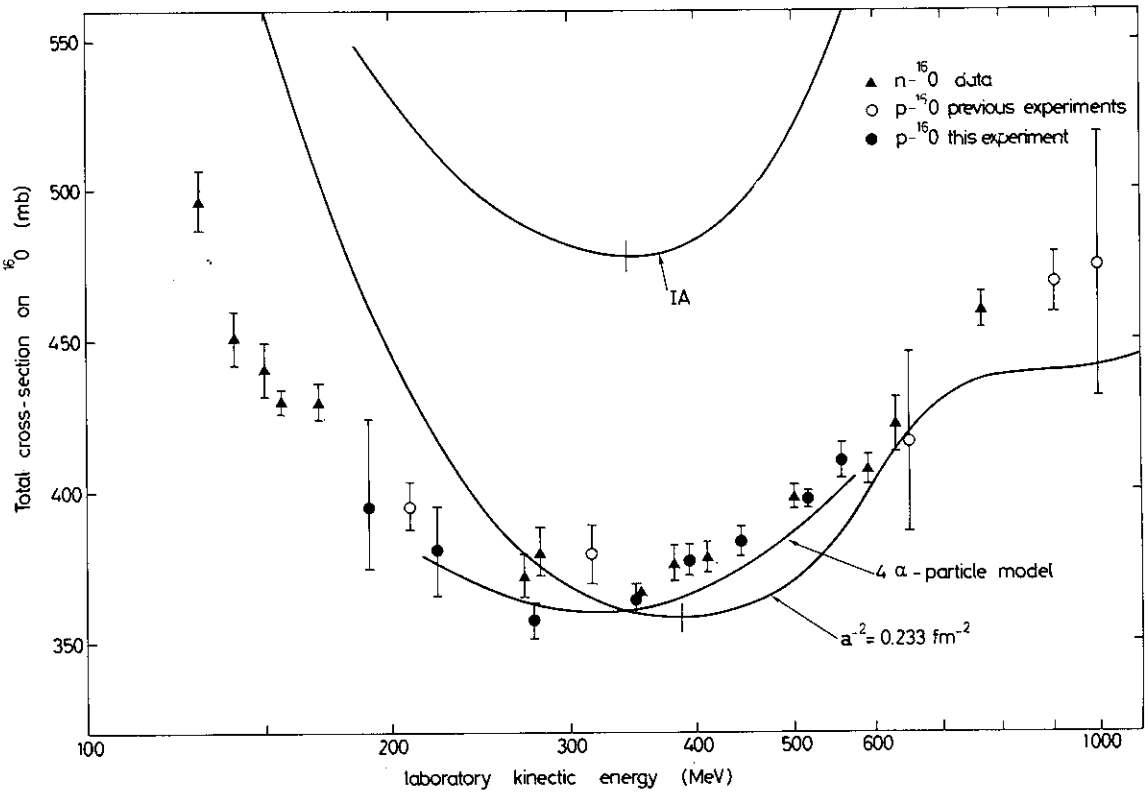

Fig. 20 Nucleon-oxygen total cross-sections; the solid curves represent Glauber model calculations.

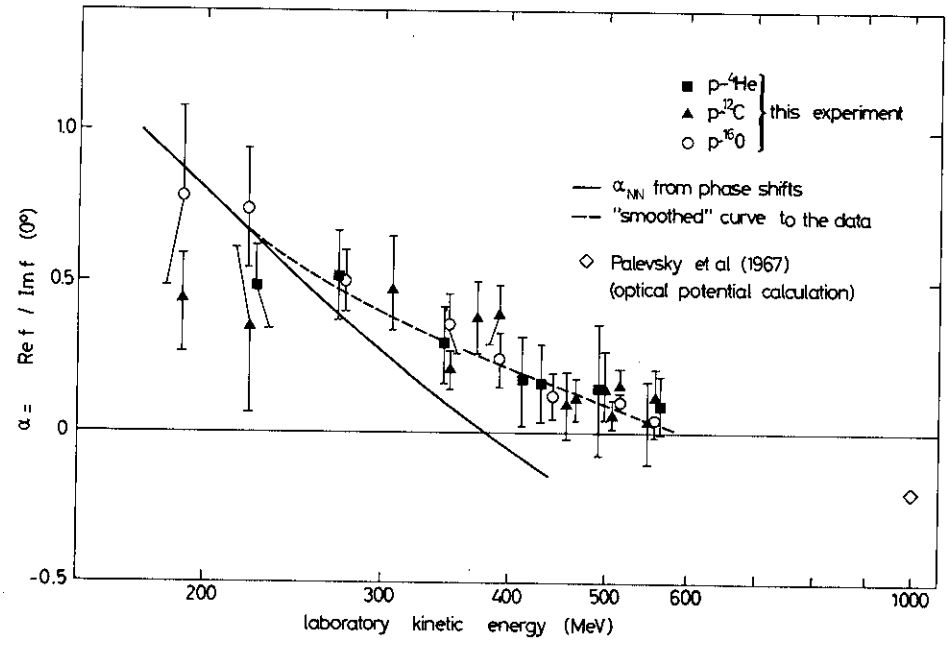

Fig. 21 Ratio of the real to the imaginary part of the spin-independent forward scattering amplitude on He, C, and O

5.2 Discussion

5.2.1 Nucleon-nucleon total cross-sections

In Fig. 16 our pp total cross-section results are compared to the prediction for total neutron-neutron cross-sections obtained from the energy-dependent Livermore phase-shift solution X [1] (the solid curve). Below 400 MeV we note an agreement within experimental errors. The Livermore analysis did not consider any pp total cross-sections as input; hence this experiment provides a direct test on the validity of the phases. In particular, it proves by the optical theorem that this set of phase shifts predicts the correct imaginary part of the spin-independent forward scattering amplitude.

Moreover, the Coulomb-nuclear interference correction in our data evaluation was based on Livermore phases. It is proportional to the real part of the spin-independent forward amplitude, and considerably influences the extrapolation to the total cross-section at zero solid angle (see Table 7, column 4; see also Fig. 12). With the above-mentioned agreement between total cross-sections the experiment is also a test for this correction and confirms, with much less precision of course, that the real part of the spin-independent forward amplitude obtained by phase shifts has the correct order of magnitude.

Above 400 MeV, where the interference correction is neglible, we found that our data lie 2% to 3% higher than the phase-shift results. This is not surprising since pion production starts around 300 MeV, which requires complex phase shifts. Various phase-shift solutions are possible because of the poor elastic scattering data.

We disagree with the data of Bugg et al.[28] at 515 MeV by about 2.4 mb (7.5%), of which approximately 0.75 mb is due to the difference in the interference correction. Bugg has based his calculation on forward dispersion relations[19], whereas we have used a more phenomenological approach. We note that the use of phase shifts to determine the Coulomb-nuclear interference has also been used in the measurement of pion-proton total cross-sections from 70 to 290 MeV [29].

5.2.2 Calculation of p-nucleus σ_{tot} by Glauber theory

Multiple scattering theory has been applied extensively during the last few years and successfully describes the structure of pion- or proton-nucleus differential cross-sections at high energies, in the limit of geometrical optics

$$kR \gg 1 ,$$

where R is the r.m.s. radius of the nucleus, and k is the beam momentum. Wilkin[30] has investigated the low-energy region where the model would be expected to break down. He performed calculations with pions of 100-300 MeV on isospin-zero nuclei such as He, C, O; kR is then of the order of 2. Surprisingly, the model still works reasonably well.

A somewhat different situation arises when scattering nucleons on nuclei. At medium energies (150 to 1000 MeV or 550 to 1700 MeV/c), spin effects, which are usually neglected in the theory, are very important when calculating differential cross-sections at small scattering angles. However, it seems worth while to calculate the forward scattering amplitude. The imaginary part is related by the optical theorem to the total cross-section and can be checked directly by experimental data.

Measured total cross-sections as a function of energy E show a minimum around 300 MeV; the rise towards high energies is due to the onset of pion production. We have checked whether the theory is capable of reproducing the position of this minimum as well as the general shape of $\sigma_{tot}(E)$ in D, He, C, and O.

With the simplest possible assumptions listed below, the total cross-section is given as a sum over A multiple scattering terms[31]:

$$\sigma_A(E) = 2\pi\, a^2\left[1 + 2a^{-2}\,\gamma^2(E)\right] \sum_{m=1}^{A} \binom{A}{m} (-1)^{m+1} \frac{1}{m} \times \left[\frac{\sigma(E)}{2\pi\, a^2\left[1 + 2a^{-2}\,\gamma^2(E)\right]}\right]^m \mathrm{Re}\left[1 - i\alpha(E)\right]^m \qquad (52)$$

$$= A \cdot \sigma - \frac{A(A-1)}{8\pi} \frac{\sigma^2}{a^2\left(1 + 2a^{-2}\gamma^2\right)} \left(1 - \alpha^2\right) + \dots , \qquad (53)$$

where A = number of nucleons in the target nucleus. (The notation differs slightly from that in Ref. 31 in order not to mix the variables in this report.)

The input quantity in the theory is the isospin averaged spin-independent nucleon-nucleon amplitude when one is calculating the scattering of nucleons on an isospin-zero target:

$$f_{NN} = \tfrac{1}{2}\left(f_{pp} + f_{pn}\right) = \tfrac{3}{4} f(I = 1) + \tfrac{1}{4} f(I = 0) \qquad (54)$$

which is approximated by an exponential in t:

$$f_{NN}(E) = \frac{ik}{4\pi}\, \sigma(E)\left[1 - i\alpha(E)\right] e^{-\gamma^2(E)\left(|t|/2\right)} \qquad (55)$$

$$\sigma = \sigma_{NN} = \tfrac{1}{2}\left(\sigma_{pp} + \sigma_{np}\right) = \tfrac{3}{4}\sigma(I = 1) + \tfrac{1}{4}\sigma(I = 0)$$

isospin averaged NN total cross-section

$$\alpha = \alpha_{NN} = \mathrm{Re}\, f_{NN}/\mathrm{Im}\, f_{NN}$$

$$\gamma^2 = \text{slope parameter} .$$

The target is considered to be a pure s-state nucleus, i.e. each nucleon has an harmonic oscillator wave function in the s-state with respect to the centre-of-mass of the nucleus. Assuming no correlations between the nucleons, the density function of the scatterer A is factorizable:

$$\rho(\vec{r}_1 \cdots \vec{r}_A) = \rho(\vec{r}_1) \cdots \rho(\vec{r}_A) = \left(\frac{1}{\pi a^2}\right)^{\frac{3}{2}} \exp\left\{-\frac{1}{a^2}\left[\sum_{i=1}^{A} r_i^2\right]\right\} , \tag{56}$$

where a is related to the r.m.s. radius R of the nucleus by

$$a^2 = \frac{2}{3} R^2 \tag{57}$$

(R values are listed in Section 4.1.1).

Total cross-sections on D, He, C, and O in the energy range 150-2000 MeV (550-2800 MeV/c) were computed with the following input data:

i) Isospin averaged total nucleon-nucleon cross-section $\sigma_{tot}(NN)$: Figure 22 shows the actual experimental situation for nucleon-nucleon total cross-section data. At low energies (< 400 MeV) we used the values obtained from Livermore phases. They agree perfectly well with our data $\sigma_{tot}(pp)$ and also represent a good mean of all existing np experimental data (for the sake of clarity, some of these have been omitted from the figure). At higher energies we took the very precise and most recent Cambridge-Rutherford (C-R) pp data and the Princeton (PPA) np data[27,32]. The faint dip in the np cross-section at 900 MeV is due to the minimum of $\sigma_{tot}(I = 0)$.

ii) α_{NN}: We considered the "smoothed" curve $\alpha(E)$ in Fig. 21 to be the best actual data for α_{NN} below 600 MeV. At higher energies it can be seen from differential cross-section calculations with Glauber theory that $|\alpha|$ may be about 0.3 at 1 GeV [30]. Furthermore, Palevsky et al.[33] performed optical model calculations using proton elastic scattering data on H, He, C, and O at 1 GeV. They found that the real part of the optical potential U is repulsive, i.e.

$$\alpha = \frac{\text{Re } U}{\text{Im } U} \sim -0.2 . \tag{58}$$

We note that α_{NN} influences only the higher-order terms in Eq. (53). The total cross-section calculation is not very sensitive to α as long as $|\alpha|$ is small with respect to 1:

example: $\sigma_{tot}(He)$ at 600 MeV

$\alpha = 0$ $\quad \sigma_{tot} = 118.9$ mb

$|\alpha| = 0.3$ $\quad \sigma_{tot} = 120.2$ mb .

We believe that $|\alpha|$ will stay smaller than 0.3 above 600 MeV. We neglect effects of about one or two per cent in σ_{tot} and therefore assume the amplitude to be pure imaginary.

iii) Slope parameter γ^2: The slope parameter γ^2 at zero momentum transfer has been taken from phase shifts up to 450 MeV. At higher energies a mean $\gamma^2 \approx 0.3$ fm^2 fits experimental data compiled by Lasinski et al.[34] rather well (Fig. 23).

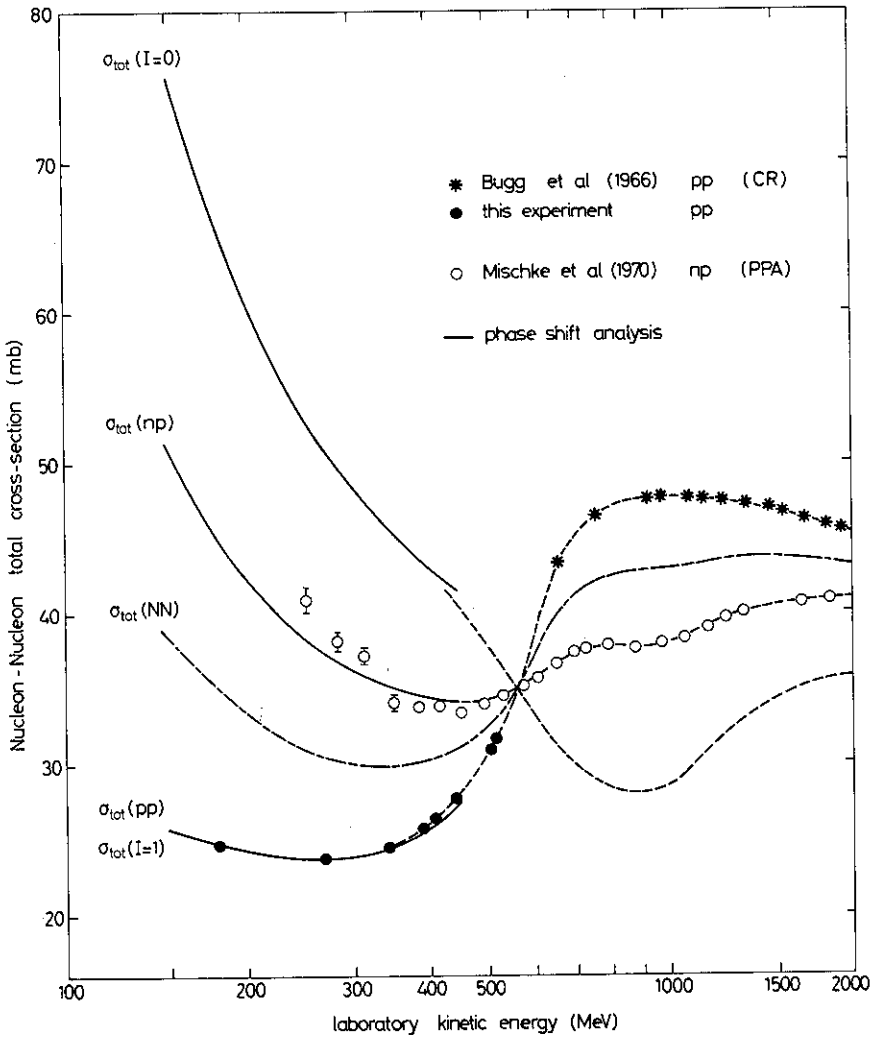

Fig. 22 Nucleon-nucleon total cross-sections

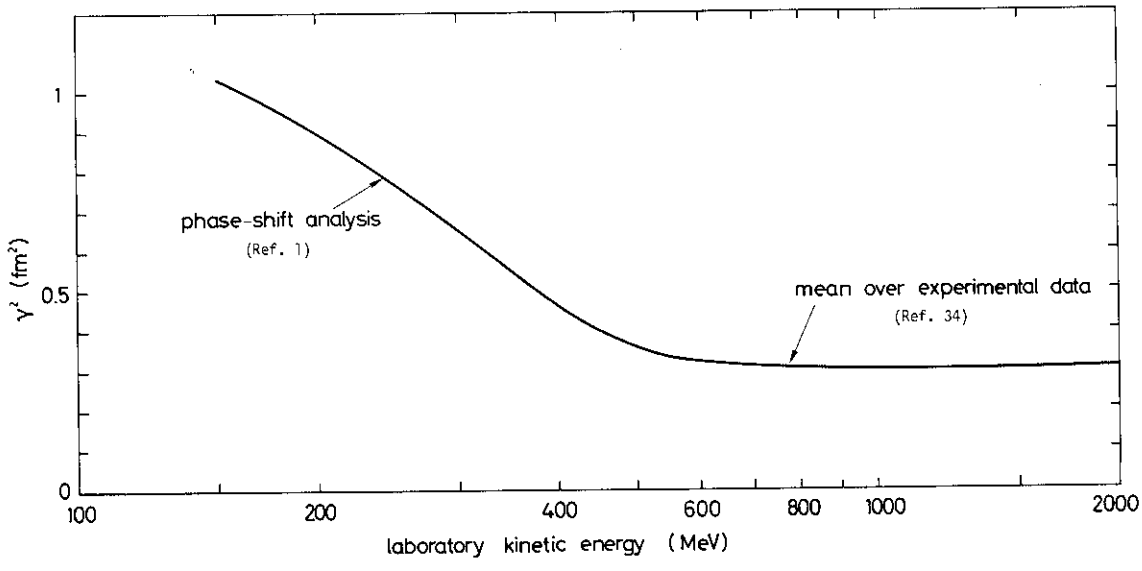

Fig. 23 Slope parameter of the spin-independent isospin averaged nucleon-nucleon amplitude

The results of the calculations are plotted in Figs. 17, 18, 19, and 20, as follows.

σ_{tot} p-d (Fig. 17): In this case formula (52) reduces simply to

$$\sigma_d = 2\sigma - \frac{1}{4\pi}\,\sigma^2(1-\alpha^2)\,\frac{a^{-2}}{(1+2a^{-2}\gamma^2)} \quad . \tag{59}$$

Instead of using c.m. coordinates to locate the position of the nucleons in the nucleus, the deuteron can be described with one coordinate only, the separation s of the two nucleons. Assuming again a Gaussian-type density distribution in s, the parameter a^{-2} in Eq. (59) equals the expectation value of the inverse square separation[35]: $a^{-2} = \langle s^{-2} \rangle$.

At low energies the impulse approximation (IA) fits the data almost perfectly. In any case, the double scattering correction is small ($\leq 2\%$) because both γ^2 and α increase towards low energies and therefore suppress the second term.

Furthermore, the charge exchange contribution can easily be taken into account by replacing σ^2 in the double scattering term by

$$\sigma_{pp}\,\sigma_{np} - \underbrace{\tfrac{1}{2}(\sigma_{np} - \sigma_{pp})^2}_{\text{charge exchange term}} \quad .$$

It reduces this term by about 20% at 200 MeV, 6% at 400 MeV, and has no effect at 560 MeV where $\sigma_{np} = \sigma_{pp}$.

At high energies we are faced with the situation where the nd data from the PPA group disagree by more than 2% with the pd data measured by the C-R group. A recent measurement[36] of the pd total cross-section at 3 GeV/c yields a result which is lower than the C-R set by 1.2 mb; thus we conclude that there can be a systematic error of this amount in the C-R data. The nd and pd cross-sections should be equal if charge symmetry is valid. We have varied the parameter $\langle s^{-2} \rangle$ and found that $\langle s^{-2} \rangle = 0.2$ fm^{-2} fits the C-R data remarkably well. It needs a value of 0.33 fm^{-2} in order to come closer to the PPA data. However, the over-all agreement in the whole energy region is much worse. The correct value for the mean inverse square separation $\langle s^{-2} \rangle$ is still not known; it may vary between 0.2 and 0.4 fm^{-2} [27,37].

σ_{tot} p-^{4}He, ^{12}C, ^{16}O (Figs. 18, 19, and 20): The comparison of our Glauber model calculations with experimental data shows five important facts:

i) The depths of the minima of the calculated total cross-sections equal the experimental minimum values, which is remarkable since the multiple scattering corrections compared to the impulse term (IA) are as large as 20-30%.

ii) The multiple scattering terms shift the minimum of the NN total cross-section, which is at 335 MeV, towards higher energies. This is due to the negative derivative $d\gamma^2/dE < 0$ in this energy region. The experimental minima, however, are at lower energies (280-300 MeV) and disagree with the theory by 70-100 MeV. The same theoretical approach predicts a shift towards lower energies for the π-nucleon (3,3) resonance in π-nucleus total cross-sections[38], which is observed experimentally.

iii) The theoretical curve has roughly the correct shape as a function of energy, and agrees fairly well at higher energies where any structure in NN total cross-sections disappears.

iv) The calculation reproduces exactly our data at 335 MeV, the minimum point of the NN total cross-section.

v) We have considered the ^{12}C and ^{16}O nucleus to be composed of 3 or 4 α-particles, respectively, and have introduced into the Glauber formalism a p-^{4}He amplitude similar to the expression (55). We used our experimental values of σ_{tot} and α's for p-^{4}He, whereas $\gamma^2 \simeq 1.05$ fm^2 was taken from differential cross-section data. The results reproduce the experimental data in ^{12}C and ^{16}O fairly well.

Since Glauber theory still works well at low energies (pd data, π-nucleus data) we have thought of various effects, not considered in the theory, which may explain the energy shift of total cross-section minima[39]. We have not made any detailed calculations.

- Fermi motion: We do not believe that the minima will move by 70 MeV when including Fermi motion of the nucleons in the nucleus, since the NN total cross-section curve is rather symmetric around its minimum. It just smoothes the structure. However, Fermi motion is the only possibility of influencing the impulse term $A \cdot \sigma$ in formula (53). Therefore, any energy shift has to occur by the multiple scattering terms (in general, five or six terms are necessary, except for He, where the double scattering dominates by far the higher-order terms). Since we are working at low energies we have to accept a series of rather large scattering angles, with the condition that the final momentum transfer to the nucleus is zero.

This immediately implies the following list of effects to be studied:

- non-Gaussian form of the elementary NN amplitude;
- strong contribution of spin effects;
- kinematical problems
- finite integration limits when integrating over the momentum transfer q;
- back-scattering;
- rescattering on the same nucleon;
- isospin 1 and 0 amplitudes have to enter the theory explicitly since they differ considerably at low energies; the α's get close to 1, i.e. delicate cancellations of higher-order terms may happen;
- non-Gaussian single-particle density in the nucleus (surface effects);
- correlations between nucleons in the nucleus.

It needs a detailed theoretical investigation in order to establish which effects contribute dominantly to the observed large energy shift. It could easily be that at different energies different effects are dominant.

5.2.3 Charge symmetry

A direct test on charge or isospin symmetry is possible by comparing proton and neutron total cross-sections on an isospin-zero target as a function of energy.

Since charge symmetry is believed to hold by 0.5% to 1% [40] it needs rather high precision data in order to be sensitive to such small differences. At present it is a difficult task to measure proton total cross-sections to an accuracy of better than 0.5% since the biggest uncertainties are still due to Coulomb and Coulomb-nuclear interference corrections at least in the energy region of a few hundred MeV. When new differential cross-

section data become available, the situation may change. For neutron total cross-sections, more often the problem of statistics and systematic errors in the apparatus of the order of 0.5-1% become important.

With the actual precision of total cross-sections on nuclei such as ^{12}C or ^{16}O it is only possible to conclude that charge symmetry is valid to about 4%. However, our data on the deuteron agree, within error, with the most recent PPA nd total cross-sections; hence charge symmetry is confirmed to about 2% (Fig. 17). We conclude that the big discrepancy of more than 2% at higher energies is probably due to systematic errors in the experiments.

5.2.4 Forward dispersion relations (FDR) on ^4He

Our experimental results on total cross-sections and the real parts of the nucleon-^{4}He scattering amplitude have stimulated an extension of a previous FDR analysis[41] to higher energies.

We quote only the results of Ref. 2 where a subtracted dispersion relation of the following form was used:

$$\mathrm{Re}\, f(E) = f(0) + \frac{k^2}{2\pi^2} P \int_0^\infty \frac{\sigma(k')\, dk'}{k'^2 - k^2} + \sum_j \frac{r_j E}{E_j(E - E_j)} , \tag{60}$$

where E and k are the laboratory kinetic energy and momentum respectively. f(0) is the subtraction constant at threshold and essentially the scattering length.

The second term is the dispersion integral extended over the physical region, experimental total cross-sections being input data. The sum over poles represents the contribution of the unphysical region; possible cuts are approximated by effective poles with the strength r_j and the position E_j.

The two terms in the physical region are known rather accurately. This allows one to form the discrepancy function $\Delta(E)$

$$\Delta(E) = \mathrm{Re}\, f_{exp}(E) - \underset{\substack{\mathrm{FDR} \\ \text{phys. region}}}{\mathrm{Re}\, f} \approx \sum_j \frac{r_j E}{E_j(E - E_j)} . \tag{61}$$

It represents direct information on the unphysical region in the limited energy intervals where values for Re f_{exp} are available (from phase shifts below 50 MeV; from Coulomb-nuclear interference at medium energies).

At low energies (E < 50 MeV), "non-relativistic" exchange processes are the dominant terms in the unphysical region, i.e. the ^{3}He pole at E_0 = -15 MeV (fixed by the neutron binding energy) with its residue r_0 and the unbound three-nucleon exchange (pd and ppn), the cuts starting at about -20 MeV:

$$\Delta(E) \simeq \frac{r_0 E}{E_0(E - E_0)} + \frac{r_1 E}{E_1(E - E_1)} . \tag{62}$$

Since E_1 (the position of the effective pole of the three-nucleon exchange) sits rather close to E_0, the analysis at low energies[41] was limited in precision and gave large errors on the residue r_0 and r_1.

At medium energies (200-600 MeV) FDR analysis becomes sensitive to "relativistic" effects, i.e. meson + 3 baryon exchange processes, which start at about -120 MeV. Again an effective pole was used to approximate this cut:

$$\frac{r_M E_M}{E_M(E - E_M)} \quad .$$

In the limit $E \gg E_0, E_1$, the "non-relativistic" pole contribution (62) simply reduces to a constant $c \sim (r_0/E_0) + (r_1/E_1)$. A least squares fit to our real parts gave the three unknown parameters r_M, E_M, and c. The constraint c helped to bring about a drastic reduction of the errors on the ^{4}He-^{3}He n coupling constant r_0 and the strength of the three-nucleon exchange r_1.

We quote the final best fit parameters:

$$E_0 = -15.4 \text{ MeV (fixed)}, \qquad r_0 = 3.2 \pm 0.4$$
$$E_1 = -53 \pm 11 \text{ MeV}, \qquad r_1 = -5.8 \pm 1.5$$
$$E_M = -600 \pm 100 \text{ MeV}, \qquad r_M = -36.5 \pm 9 \quad .$$

Figure 24 illustrates the different contribution of this FDR analysis to the Re f.

If one relies on the optical potential prediction for α at 1 GeV incident kinetic energy[33] where α is about -0.2, it is not yet possible to indicate at what energy Re f changes its sign. With the three-pole fit in this FDR analysis, one recognizes that the contribution from the physical region is opposite in sign to the summed pole terms but about equal in magnitude. One is faced with delicate cancellations; thus the calculated energy where Re f equals zero depends strongly on the way in which one parametrizes the unphysical region.

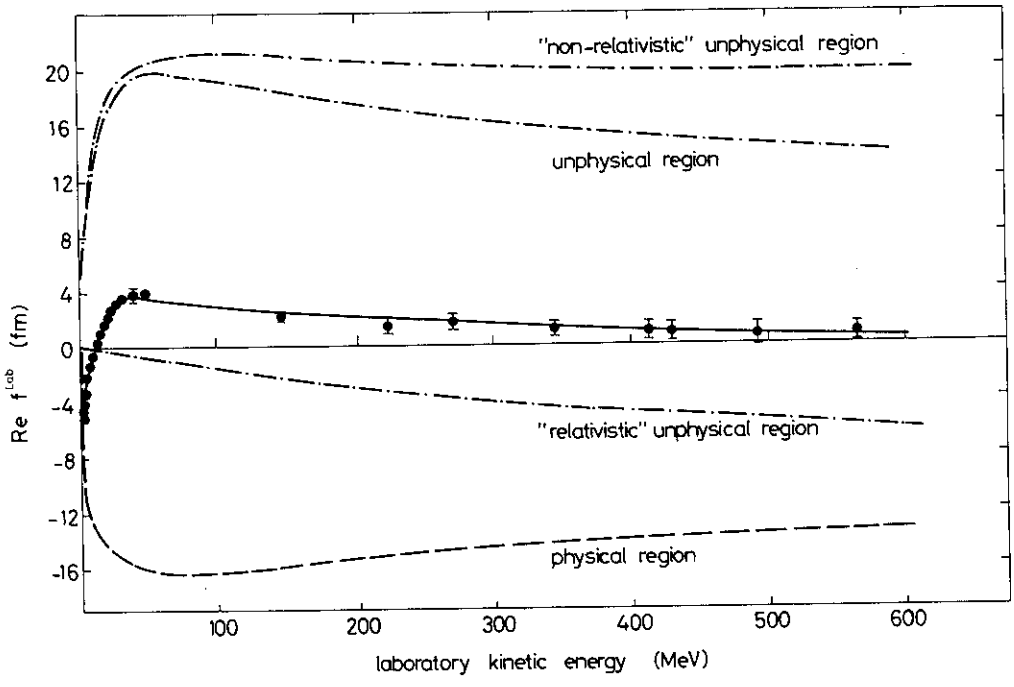

Fig. 24 Re f in ^{4}He; forward dispersion relation analysis

Acknowledgements

We are very grateful to Dr. E.G. Michaelis, Leader of the CERN MSC Division, for his interest and support given to us in carrying out this work.

We wish to thank Professors J.P. Blaser (ETH, Zurich) and R. Bouchez (University of Grenoble) who have given four of us (P.S., M.P. and B.F., C.S.,) the opportunity of working at CERN.

We appreciate deeply various fruitful discussions with Dr. M.P. Locher.

REFERENCES

1) M.H. MacGregor, R.A. Arndt and R.M. Wright, Phys. Rev. 182, 1714 (1969).

2) M.P. Locher, Nuclear Phys. B36, 634 (1972).

3) R.D. Miller, D.C. Sewell and R.W. Wright, Phys. Rev. 81, 374 (1951).

4) P.U. Renberg, D.F. Measday, M. Pepin, P. Schwaller, B. Favier and C. Richard-Serre, Nuclear Phys. A183, 81 (1972).

5) R.J. Tapper, NIRL/R/95 (1965).

6) R.B. Stewart and V.J. Johnson (eds.), Compendium of properties of materials at low temperature, technical report 60-56, part 1, Wright Air Development Division, Wright Patterson Air Force Base, Ohio.

7) C. Serre, CERN 67-5 (1967).

8) J.F. Janni, Air Force Weapons Laboratory Technical report AWFL-TR-65-150 (1966).

9) W.H. Barkas and M.J. Berger, NAS-NRC publication 1133 (1964).

10) G. Molière, Z. Naturforsch. 3a, 78 (1948).

11) H.A. Bethe, Phys. Rev. 89, 1256 (1953).

12) H. Øverås, CERN 63-9 (1963).

13) G.J. Marmer, ANL-HEP 6801 (1968).

14) A.M. Cormack, Nuclear Phys. 52, 286 (1964).

15) U. Fano, Phys. Rev. 93, 117 (1954).

16) J. Raynal, Nuclear Phys. 28, 220 (1961).

17) L.D. Solov'ev, Soviet Phys. JETP 22, 205 (1966).

18) H.A. Bethe, Ann. Phys. 3, 190 (1958).

19) P. Söding, Phys. Letters 8, 285 (1964).

20) A.A. Carter and D.V. Bugg, Phys. Letters 20, 203 (1966).

21) L.M.C. Dutton, R.J.W. Howells, J.D. Jafar and H.B. van der Raay, Phys. Letters 25 B, 245 (1967).
L.M.C. Dutton and H.B. van der Raay, Phys. Letters 26 B, 679 (1968).

22) P. Signell and J. Holdeman, Phys. Rev. Letters 27, 1393 (1971).

23) G. Giacomelli, CERN-HERA 69-3 (1969).

24) V.S. Barashenkov, Interaction cross-sections of elementary particles (1968) (English translation: IPST Press, Jerusalem).

25) J.D. Hansen, D.R.O. Morrison, N. Tovey and E. Flamino CERN-HERA 70-2 (1970).

26) O. Benary, Le Roy R. Price and G. Alexander, UCRL-20000 NN (1970).

27) A.H. Cromer and J.N. Palmieri, Ann. Phys. 30, 32 (1964).

28) D.V. Bugg, D.C. Salter, G.H. Stafford, R.F. George, K.F. Riley and R.J. Tapper, Phys. Rev. 146, 980 (1966).

29) A.A. Carter, J.R. Williams, D.V. Bugg, P.J. Bussey and D.R. Dance, Nuclear Phys. B26, 445 (1971).

30) C. Wilkin, Proceedings of the Banff Summer School on Intermediate Energy Nuclear Physics (Aug 1970) (published by the Department of Physics, the University of Alberta, Canada).

31) B. Margolis and C.S. Lam, Nuclear and particle physics (W.A. Benjamin, Inc., New York, 1968), p. 469.

32) R.E. Mischke, T.J. Devlin, W. Johnson, J. Norem, K. Vosburgh and W. Schimmerling, Phys. Rev. Letters 25, 1724 (1970).

33) H. Palevsky, J.L. Friedes, R.J. Sutter, G.W. Bennett, G.I. Igo, D.W. Simpson, G.C. Phillips, D.M. Corley, N.S. Wall, R.L. Sterns and B. Gottschalk, Phys. Rev. Letters 18, 1200 (1967).

34) T. Lasinski, R. Levi Setti, B. Schwarzschild and P. Ukleja, Nuclear Phys. B37, 1, (1972).

35) V. Franco and R.J. Glauber, Phys. Rev. 142, 1195 (1966).

36) R.J. Abrams, R.L. Cool, G. Giacomelli, T.F. Kycia, B.A. Leontic, K.K. Li and D.N. Michael, Phys. Rev. D1, 2477 (1970).

37) A.A. Carter, K.F. Riley, R.J. Tapper, D.V. Bugg, R.S. Gilmore, K.M. Knight, D.C. Salter, G.H. Stafford, E.J.N. Wilson, J.D. Davies, J.D. Dowell, P.M. Hattersley, R.J. Homer and A.W. O'Dell, Phys. Rev. 168, 1457 (1968).

38) M.P. Locher, O. Steinmann and N. Straumann, Nuclear Phys. B27, 598 (1971).

39) T.E.O. Ericson, K. Gottfried, O. Kofoed-Hansen, M.P. Locher and C. Wilkin, private communication.

40) E.M. Henley, Isospin in nuclear physics (Ed. D.H. Wilkinson) (North-Holland Publishing Company, Amsterdam, 1969).

41) T.E.O. Ericson and M.P. Locher, Nuclear Phys. A148, 1 (1970).